2011

Design and analysis of a titanium/nanocomposite pressure vessel for aerospace applications

Roosevelt Wright

DESIGN AND ANALYSIS OF A TITANIUM/NANOCOMPOSITE PRESSURE VESSEL FOR AEROSPACE APPLICATIONS

by

ROOSEVELT WRIGHT

A THESIS

Submitted in partial fulfillment of the requirements
for the degree of Master of Science in Engineering
in
The Department of Mechanical and Aerospace Engineering
to
The School of Graduate Studies
of
The University of Alabama in Huntsville

HUNTSVILLE, ALABAMA

2011

In presenting this thesis in partial fulfillment of the requirements for a master's degree from The University of Alabama in Huntsville, I agree that the Library of this University shall make it freely available for inspection. I further agree that permission for extensive copying for scholarly purposes may be granted by my advisor or, in his absence, by the Chair of the Department or the Dean of the School of Graduate Studies. It is also understood that due recognition shall be given to me and to The University of Alabama in Huntsville in any scholarly use which may be made of any material in this thesis.

Ronald Hunt 3-17-2011

(student signature) (date)

THESIS APPROVAL FORM

Submitted by Roosevelt Wright in partial fulfillment of the requirements for the degree of Master of Science in Engineering and accepted on behalf of the Faculty of the School of Graduate Studies by the thesis committee.

We, the undersigned members of the Graduate Faculty of the University of Alabama in Huntsville, certify that we have advised and/or supervised the candidate on the work described in this thesis. We further certify that we have reviewed the thesis manuscript and approve it in partial fulfillment of the requirements for the degree of Master of Science in Engineering.

03/11/2011 Committee Chair
(Date)

3/11/11

3/11/11

Robert A Frederick Jr. Department Chair

R.M. Hyshida for S. Mahalingam 3/14/11 College Dean

Rhonda Kay Gaede 4/25/11 Graduate Dean

ABSTRACT
The School of Graduate Studies
The University of Alabama in Huntsville

Degree Master of Science in Engineering College/Dept. Engineering/Mechanical and Aerospace Engineering

Name of Candidate Roosevelt Wright
Title Design and Analysis of a Titanium/Nanocomposite Pressure Vessel for Aerospace Applications

This thesis reports the results of a preliminary design of a nanocomposite overwrapped pressure vessel (NOPV). The NOPV consists of a titanium liner helically overwrapped with a Polyacrylonitrile (PAN) Single-Walled Carbon Nanotube (SWCNT) fiber in an epoxy matrix. Micromechanics models were used to predict the mechanical properties of the PAN-SWCNT/EPOXY composites. A MATLAB code based on an elasticity solution was developed to analyze the stresses and deformations of multilayered filament wound pressure vessels under internal pressure. A case study on the helium pressurization tank used in the National Aeronautics and Space Administration's (NASA) Jet Propulsion Laboratory (JPL) Messenger Spacecraft was performed to assess the nanocomposite performance. Comparisons between the Toray 1000 advanced filament composites currently in use and the proposed nanocomposites were made. The study shows that the NOPV offers advantages in mass reduction. Such reduction is a common goal in aerospace design. In addition, parametric studies were also conducted to determine the optimal configuration of the proposed NOPV.

Abstract Approval: Committee Chair 

Department Chair 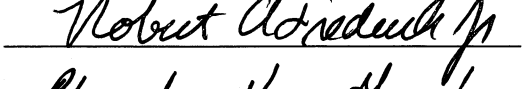

Graduate Dean 

ACKNOWLEDGMENTS

This thesis was completed under the encouragement and guidance of my advisors, Dr. Mark Lin, Dr. John Gilbert and Dr. Q. H. Ken Zuo, who have given me support during this research. I would personally like to thank Dr. Lin, who has generously given me his experience in mechanical engineering design. Since the moment I met Dr. Lin, I have felt his unconditional support and confidence and now is the time to say thank you. Dr. Lin has served as a role model for the type of engineer I aspire to become. I would like to thank the late Dr. Mark Bower for providing me with some of the skills I needed and constant words of encouragement. Finally, I would like to thank all of my family who have sacrificed for my education.

TABLE OF CONTENTS

LIST OF FIGURES

LIST OF TABLES

CHAPTER 1

INTRODUCTION AND OBJECTIVE

1.1 Composite Pressure Vessels

Composite Overwrapped Pressure Vessels (COPVs) are used in many aerospace applications. Often, a COPV is used to store an inert gas used in blow-down rocket propulsion systems. Figure 1.1 below shows such a system. The COPV is initially pressurized with an inert gas located upstream in the propulsion system. When the tank valve is opened, the high-pressure gas travels to both the rocket fuel and oxidizer tanks. Such mixing downstream in a combustion chamber causes the rocket engine to generate thrust.[1]

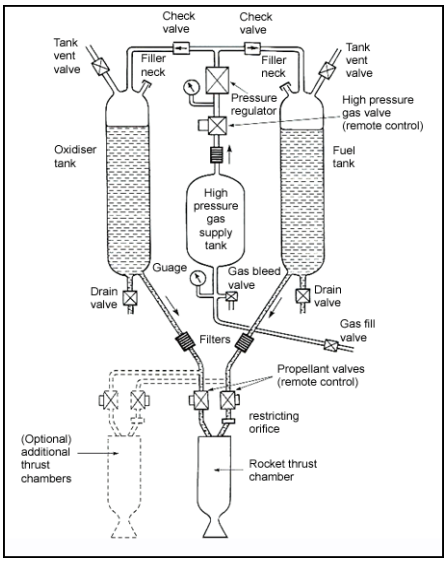

Figure 1.1 Blow-Down System Schematic[2]

The pressurization tanks are typically spherical or cylindrical; however, depending on the design requirements, alternative geometry is used. Figure 1.2 shows two fabricated composite overwrapped pressure vessels. The image on the left is a rare conical pressure vessel, whereas on the right a typical cylindrical pressure vessel with elliptical end caps.

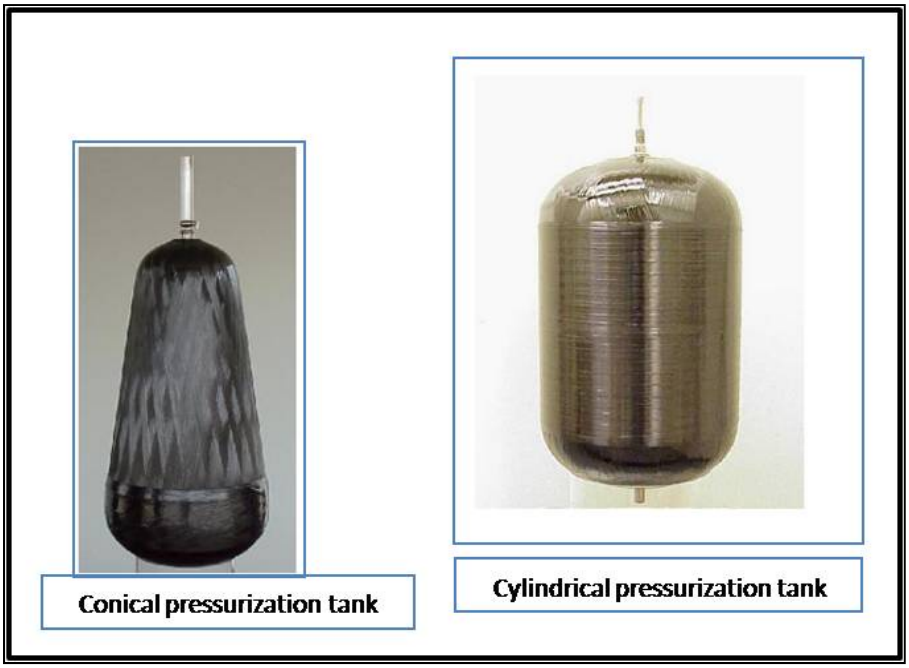

Figure 1.2 Pressurization Tanks[3,4]

Also, in order to reduce the propulsion system mass, some rocket propulsion systems use COPVs for propellant storage. These tanks are typically cylindrical with hemispherical end caps. Figure 1.3 shows a propellant tank with hoop composite wraps with exposed metallic end caps.

Figure 1.3 Propellant Tanks[5]

1.2 Single-Walled Carbon Nanotubes (SWCNT)

Single-Walled Carbon Nanotubes (SWCNTs) were invented in 1993 and have great mechanical properties.[6] SWCNTs are cylindrical structures based on the hexagonal lattice of carbon atoms that covalently bond together and form crystalline graphite. Carbon nanotubes exist as a macro-molecule of carbon, analogous to a sheet of graphite that is rolled into a seamless cylinder.[7] A carbon nanotube consisting of one rolled cylindrical graphene sheet is called a Single-Walled Carbon Nanotube.[8] Figure 1.4 illustrates a planar graphene sheet rolled to create a SWCNT. Most single-walled nanotubes (SWNT) have a diameter of close to 1 nm, with a tube length that can be many million times longer.[9]

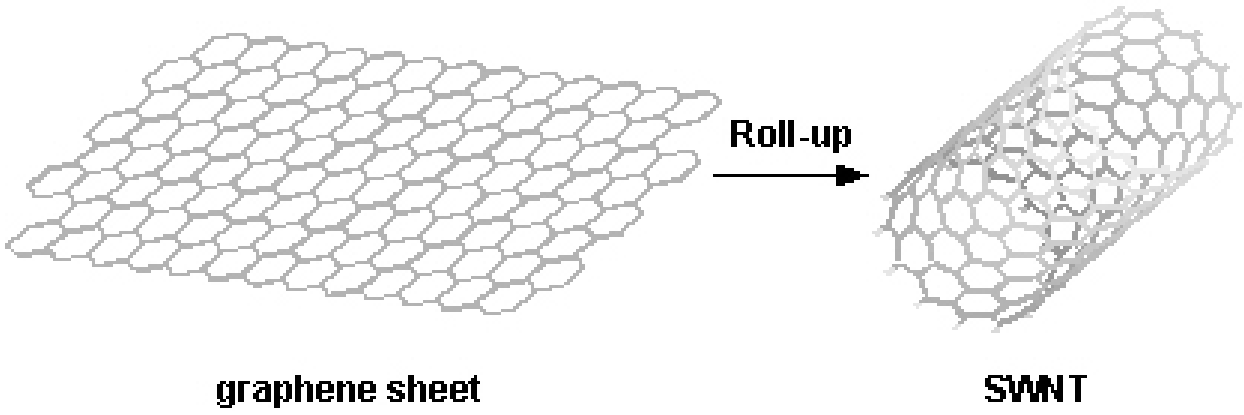

Figure 1.4 Single Wall Carbon Nanotubes[10]

1.3 Objective

The objective of this thesis is to design a Nanocomposite Over-Wrapped Pressure Vessel. The systematic approach outlined below was used to accomplish this objective:

a. Develop micromechanics models to predict the mechanical properties of the PAN-SWCNT/EPOXY composites.
b. Develop a MATLAB code based on an elasticity solution to analyze the stresses and deformations of multilayered filament wound pressure vessels under internal pressure.
c. Perform a case study on the helium pressurization tank used in NASA's JPL Messenger Spacecraft to assess the nanocomposite performance.
d. Conduct a parametric study to determine the optimal configuration of the proposed NOPV.

CHAPTER 2

PAN-SWCNT FIBER

2.1 PAN-SWCNT Fiber History

As stated previously, SWCNTs exhibit exceptional mechanical properties; however, their nano-length limits their use as stand-alone fiber reinforcement in laminated composites. The work performed by J. Liang at the Georgia Institute of Technology produced a PAN-SWCNT fiber with a longitudinal modulus of 13.6 Giga Pascal's (GPa) and tensile strength of 0.45 Mega Pascal's (MPa).[6] The SWCNT weight fraction of these PAN-SWCNT fibers was 5%.[6]

To produce PAN-SWCNT fibers, SWCNTs are acid treated in order to remove water before they are mixed with a solvent. Next, the SWCNTs are immersed in a Dimethyl Formamide (DMF) solvent, and then they are sonicated: Intense sound waves in liquid solvent are used to remove excess solvent from the SWCNTs. Later, the PAN copolymer is added and dissolved until a homogeneous dope is obtained. Afterwards, the PAN-SWCNT combination is dry-wet spun through a spinneret as shown in Figure 2.1.

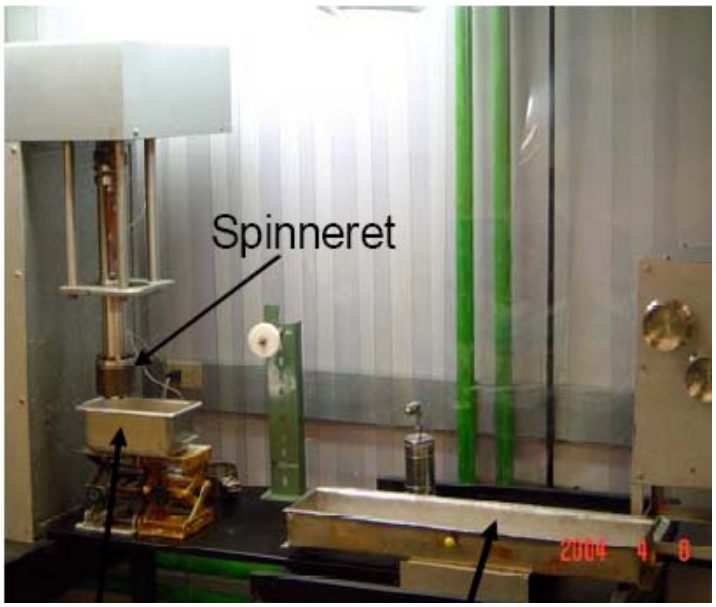

Figure 2.1 PAN-SWCNT Fiber [6]

This spinneret is an extrusion die with many holes where the PAN-SWCNT mix is forced to form the filament.[6]

2.2 PAN-SWCNT Fiber Mechanical Properties

Mechanical properties of a PAN-SWCNT fiber at 5% weight fraction are not comparable to those of traditional reinforcing fibers, such as aramid and graphite fibers, which have a typical fiber modulus of 124 GPa and 230 GPa, respectively.[11] In order to achieve better material properties for a PAN-SWCNT fiber, the volume fraction of SWCNTs was increased to 80% for this thesis. The mechanical properties of such a fiber were theoretically determined by micromechanics models.

The PAN-SWCNT fiber properties were obtained by using the Halpin-Tsai relations for unidirectional short fiber composites. Figure 2.2 illustrates the SWCNTs aligned and suspended in a PAN matrix.

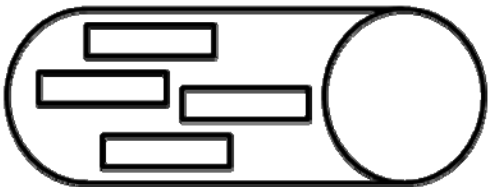

Figure 2.2 Aligned Short Fibers Embedded in PAN Matrix

The fiber stiffness in the principal direction E_{11} was approximated by Equation (2.1). Also, the in-plane shear stiffness G_{12} was approximated by Equation (2.1). As stated earlier, the volume fraction of SWCNTs was 80% and the PAN matrix 20%.

$$\frac{M}{M_m} = \frac{1+\xi\eta V_f}{1-\eta V_f}, \tag{2.1}$$

$$\eta = \frac{(M_f/M_m)-1}{(M_f/M_m)+\xi} \quad . \tag{2.2}$$

From Equation (2.1), PAN-SWCNT fiber properties become $M = E_{11}, E_{22}, G_{12}$, where $M_f = E_f, G_f$ and v_f are the SWCNT properties and $M_m = E_m, G_m$, v_m are the PAN matrix properties. The in-plane passion ratio v_f was computed with the rules of mixture relation $v_f = v_{SWNT} V_{SWNT} + v_{PAN} V_{PAN}$.[12] The PAN-SWCNT fiber transverse modulus E_{22} was also calculated using Equation (2.1). The mechanical properties used are shown in Table 2.1. The reinforcing factor ξ used for the longitudinal and transverse modulus was determined by $\xi = 2\left(\frac{l}{t}\right) + 40V_f^{10}$, $\xi = 2\left(\frac{w}{t}\right) + 40V_f^{10}$, respectively. Likewise, for the in-plane shear modulus, it is calculated by $\xi = \left(\frac{w}{t}\right)^{1.732} + 40V_f^{10}$, where w, l, and t are the reinforcement length, width, and thickness, respectively,[12] assuming that the fiber has a

circular cross section $l = l$ and $t = w = d_f$. Table 2.1 contains the properties of the constituent materials used in the Halpin-Tsai relations for unidirectional short fiber composites.

Table 2.1 SWCNT and PAN Mechanical Properties

Property	**SWCNT**	**PAN**
Axial modulus [TPa][6,11]	1	.0079
Transverse Modulus [GPa][6,11]	15	7.9
Axial Poisson's ratio [6,13]	0.17	.07
Axial shear modulus [GPa][6,13]	19.5	3.69
density [g/cm^3][6,13]	1.3	1.18

In order to verify the Halpin-Tsai model used to compute the fiber properties, a comparison between the predicted results and empirical data was performed. Using the longitudinal modulus of 13.1 ± 1MPa[6] obtained experimentally by Liang for 95/5 wt% PAN-SWCNT composite fiber, it is shown that the difference between the empirical and theoretical results is 15.6 % for the nominal modulus and 7.7 % for the minimum modulus. This relatively low percentage difference suggested that the Halpin-Tsai method agreed well with the empirical data.

The nanocomposite fiber density was calculated by using the densities of each constituent in the fiber and the known fiber volume fractions (V_f) from Table 2.1. The fiber density ρ_f was calculated by $\rho_f = \rho_{SWCNT} V_f + \rho_{PAN} (1 - V_f)$, where ρ_{SWCNT} and ρ_{PAN} are the density of the SWCNT whiskers and PAN matrix, respectively.

Table 2.2 shows the calculated fiber properties, where (l/t) and (w/t) are the length over thickness and width over thickness ratios of the SWCNTs, respectively.

Table 2.2 Fiber Properties

Property	**[PAN/SWCNT]**
Axial modulus [GPa]	282.6
Axial Poisson's ratio	0.15
Transverse Modulus [GPa]	13.4
Axial shear modulus[GPa]	14.8
Density [g/cm^3]	1.22
Specific gravity	1.22
Volume fraction	.8
l/t^2	4
w/t^2	1

CHAPTER 3

NANOCOMPOSITE HYBRID LAMINAE

The PAN-SWCNT/EPOXY lamina is considered a hybrid composite material because the constituent materials are made with two or more different materials. Literature reviews were performed to find material properties for the nanocomposites. Again, for many of the material properties, it was necessary to use micromechanics models to calculate the nanocomposite's mechanical properties. Given the properties of a heterogeneous material, micromechanics models can predict some of the material properties. A nanocomposite consists of materials that are of the scale of nanometers ($1x10^{-9}$m). The accepted range to be classified as a nanocomposite is that one of the constituents is less than 100 nm. At this scale, the properties of materials are different from those of the same bulk material. Generally, advanced composite materials have constituents on the microscale ($1x10^{-6}$m). By having materials at the nanometer scale, most of the properties of the resulting composite material are better than the ones at the microscale.[12]

3.1 Nanocomposite Hybrid Laminae Properties

Since experimental data for a 70%/30% volume fraction PAN-SWCNT/EPOXY laminae conceptualized in Figure 3.1 were not available in the open literature, micromechanics models were used to approximate the laminae stiffness.

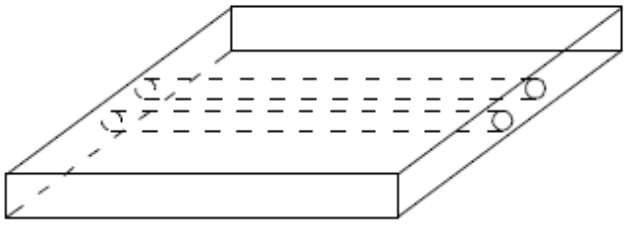

Figure 3.1 Continuous PAN-SWCNT Fiber in Epoxy Matrix

Assuming that the hybrid nanocomposite laminae meet the following conditions:[12]

- There are no voids between fibers and matrix;
- The spacing between fibers is uniform;
- All fibers run parallel and are continuous,

The longitudinal modulus E_1 of a composite material can be calculated based on the rule of mixtures by Equation (3.1).

$$E_1 = E_f V_f + E_m V_m, \tag{3.1}$$

$$E_2 = \frac{E_f E_m}{E_m V_f + E_f V_m} \tag{3.2}$$

and

$$G_{12} = \frac{G_f G_m}{G_m V_f + G_f V_m} \quad , \tag{3.3}$$

where E_f is the fiber longitudinal modulus, V_f the fiber volume fraction, E_m the matrix longitudinal modulus, and V_m the matrix volume fraction. For the current study, V_f was assumed to be 70%, and E_f was taken from the Halpin-Tsai 20%/80% volume fraction PAN/SWCNT fiber listed in Table 2.2. The stiffness of the nanocomposite laminae in the transverse fiber direction E_2, was determined using Equation (3.2). The shear modulus can be obtained from Equation (3.3),[12] where G_f and G_m are the shear modulus of the fiber and matrix, respectively. The epoxy matrix in the analysis had a Young modulus and shear modulus of 3.4 and 1.308 GPa, respectively.[11]

The major Poisson's ratio ν_{12} was also determined by using the rule of mixtures given in Equation (3.4). The variable ν_f is the major Poisson ratio of the fiber, and ν_m is the Poisson ratio of the matrix. The epoxy matrix in the analysis had a Poisson ratio[11] of 0.3, and ν_f was taken from Table 2.2. The transverse Poisson's ratio was calculated with the aid of Equation (3.5). Typically, the transverse Poisson ratio is determined empirically. However, Kirchner and Lapp recommend using Equation (3.5), for ν_{23} when data is not available.[14]

$$\nu_{12} = \nu_f V_f + \nu_m (1 - V_f) \tag{3.4}$$

and

$$\nu_{23} = \nu_f V_f + \nu_m (1 - V_f) \left[\frac{1 + \nu_m - \nu_{12}(E_m / E_1)}{1 - \nu_m^2 + \nu_m \nu_{12}(E_m / E_1)} \right] \quad . \tag{3.5}$$

A Matrix Laboratory (MATLAB) subroutine based on Equations (2.1) thru (2.2) and (3.1) thru (3.5) was created to calculate the PAN-SWCNT/ EPOXY laminae properties.

The PAN-SWCNT micromechanics model subroutine can be seen in Appendix A. The calculated laminae properties are shown in Table 3.1.

Table 3.1 Nanocomposite Hybrid Laminae Mechanical Properties

Property	**PAN-SWCNT/EPOXY**
Axial modulus [GPa]	200.8
Transverse Modulus [GPa]	11.3
Axial Poisson's ratio	0.2
Transverse Poisson's ratio	0.3
Axial shear modulus [GPa]	7.9
Fiber volume [%]	70.7
density [g/cm^3]	1.22
Specific gravity	1.22

CHAPTER 4

ELASTICITY FORMULATION FOR NOPV

4.1 Composite Layers

Treating the NOPV as a laminated cylinder and considering linear elastic response only, a displacement-based linear elastic solution method is used for the analysis of the structure. The coordinate system used in the analysis of the NOPV is depicted below in Figure 4.1.

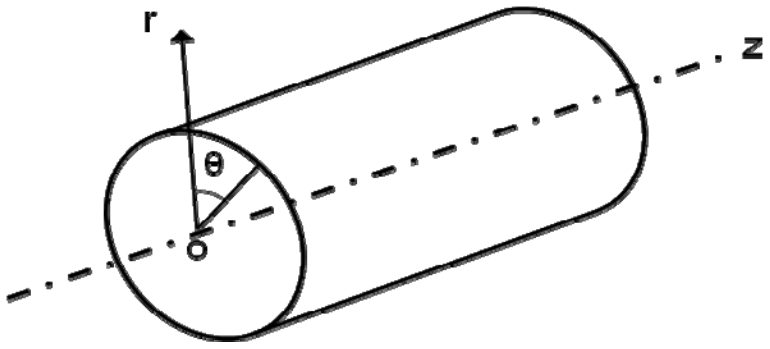

Figure 4.1 NOPV Coordinate System

Since it is a multi-layered structure, the traction and displacement are continuous at the interfaces. The following three assumptions are made.[15]

1. The cylindrical portion of the tank is assumed to be long. The analysis is valid for the sections away from the elliptical end caps, and no end effects are considered. The

loads are uniform along the axial direction. Hence, stresses and strains are independent of the axial coordinate z.

2. Stresses and strains are assumed to be independent of the circumferential coordinate è due to the nature of axis-symmetry of the applied loading and material configurations considered.

3. The composite cylinder is free to rotate about the z-axis. Due to the axis-symmetry of the applied mechanical loads, the cylinder deforms axisymmetrically and keeps its circular shape unchanged. Consequently, radial displacement is a function of the radial coordinate r only, while the cross section can rotate about the z-axis.

Based on these assumptions, the displacement fields in the radial, circumferential, and axial directions can be expressed as $u_r = u_r(r)$, $u_\theta = u_\theta(r,z)$, and $u_z = u_z(z)$, respectively.

With the absence of body forces, the equilibrium relations for the k^{th} laminae can be written in terms of cylindrical coordinates (r,θ,z) [16] as

$$\frac{\partial \sigma_r^{(k)}}{\partial r} + \frac{1}{r}\frac{\partial \tau_{\theta r}^{(k)}}{\partial \theta} + \frac{\partial \tau_{zr}^{(k)}}{\partial z} + \frac{\sigma_r^{(k)} - \sigma_\theta^{(k)}}{r} = 0, \tag{4.1}$$

$$\frac{\partial \tau_{\theta r}^{(k)}}{\partial r} + \frac{1}{r}\frac{\partial \sigma_\theta^{(k)}}{\partial \theta} + \frac{\partial \tau_{z\theta}^{(k)}}{\partial z} + \frac{2\tau_{\theta r}^{(k)}}{r} = 0, \tag{4.2}$$

and

$$\frac{\partial \tau_{zr}^{(k)}}{\partial r} + \frac{1}{r}\frac{\partial \tau_{z\theta}^{(k)}}{\partial \theta} + \frac{\partial \sigma_z^{(k)}}{\partial z} + \frac{\tau_{zr}^{(k)}}{r} = 0. \tag{4.3}$$

Since the PAN-SWCNT/EPOXY pressure vessel can be treated as a composite circular cylindrical under axisymmetric loading,[15] the terms involving $\frac{\partial}{\partial\theta}$ vanish.

Thus, the equilibrium equations become

$$\frac{\partial\sigma_r^{(k)}}{\partial r}+\frac{\sigma_r^{(k)}-\sigma_\theta^{(k)}}{r}=0, \tag{4.4}$$

$$\frac{\partial\tau_{\theta r}^{(k)}}{\partial r}+\frac{2\tau_{\theta r}^{(k)}}{r}=0, \tag{4.5}$$

and

$$\frac{\partial\tau_{zr}^{(k)}}{\partial r}+\frac{\tau_{zr}^{(k)}}{r}=0. \tag{4.6}$$

The engineering strain and displacement relations in cylindrical coordinates are written as

$$\varepsilon_r^{(k)}=\frac{\partial u_r^{(k)}}{\partial r}, \tag{4.7}$$

$$\varepsilon_\theta^{(k)}=\frac{1}{r}\frac{\partial u_\theta^{(k)}}{\partial\theta}+\frac{u_r^{(k)}}{r}, \tag{4.8}$$

$$\varepsilon_z^{(k)}=\frac{\partial u_z^{(k)}}{\partial z}, \tag{4.9}$$

$$\gamma_{z\theta}^{(k)}=\frac{1}{r}\frac{\partial u_z^{(k)}}{\partial\theta}+\frac{\partial u_\theta^{(k)}}{\partial z}, \tag{4.10}$$

$$\gamma_{zr}^{(k)}=\frac{\partial u_z^{(k)}}{\partial r}+\frac{\partial u_r^{(k)}}{\partial z}, \tag{4.11}$$

$$\gamma_{\theta r}^{(k)}=\frac{1}{r}\frac{\partial u_r^{(k)}}{\partial\theta}+r\frac{\partial}{\partial r}\left(\frac{u_\theta^{(k)}}{r}\right), \tag{4.12}$$

where $\varepsilon_r^{(k)}$ is the radial strain, $\varepsilon_\theta^{(k)}$ the hoop strain, and $\varepsilon_z^{(k)}$ the axial strain, $\gamma_{z\theta}^{(k)}$ and $\gamma_{zr}^{(k)}$ the transverse shear strains, and $\gamma_{\theta r}^{(k)}$ the in-plane shear strain.

From the stated assumptions, the strain-displacement[16] reduce to [15]

$$\varepsilon_\theta^{(k)} = \frac{u_r^{(k)}}{r}, \tag{4.13}$$

$$\varepsilon_z^{(k)} = \varepsilon_0, \tag{4.14}$$

$$\gamma_{z\theta}^{(k)} = \gamma_0 r, \tag{4.15}$$

$$\gamma_{zr}^{(k)} = 0, \tag{4.16}$$

$$\gamma_{\theta r}^{(k)} = 0, \tag{4.17}$$

where ε_0 and γ_0 are the constant axial strain and constant twist rate, respectively.

Since there is one plane of material symmetry, the constitutive relations for the general monoclinic lamina take the form of [15]

$$\begin{Bmatrix} \sigma_z \\ \sigma_\theta \\ \sigma_r \\ \tau_{\theta r} \\ \tau_{rz} \\ \tau_{z\theta} \end{Bmatrix}^{(k)} = \begin{bmatrix} \overline{C_{11}} & \overline{C_{12}} & \overline{C_{13}} & 0 & 0 & \overline{C_{16}} \\ \overline{C_{12}} & \overline{C_{22}} & \overline{C_{23}} & 0 & 0 & \overline{C_{26}} \\ \overline{C_{13}} & \overline{C_{23}} & \overline{C_{33}} & 0 & 0 & \overline{C_{36}} \\ 0 & 0 & 0 & \overline{C_{44}} & \overline{C_{45}} & 0 \\ 0 & 0 & 0 & \overline{C_{54}} & \overline{C_{55}} & 0 \\ \overline{C_{16}} & \overline{C_{26}} & \overline{C_{36}} & 0 & 0 & \overline{C_{66}} \end{bmatrix}^{(k)} \begin{Bmatrix} \varepsilon_z \\ \varepsilon_\theta \\ \varepsilon_r \\ \gamma_{\theta r} \\ \gamma_{rz} \\ \gamma_{z\theta} \end{Bmatrix}^{(k)} . \tag{4.18}$$

Integrating Equations (4.5) and (4.6), the transverse shear stress components[15] can be obtained as

$$\tau_{r\theta} = \frac{A^{(k)}}{r^2}, \tag{4.19}$$

$$\tau_{rz} = \frac{B^{(k)}}{r}, \tag{4.20}$$

where $A^{(k)}$ and $B^{(k)}$ are constants to be determined. Applying the traction boundary condition for N laminae at the outer radial surface, i.e., $\tau_{r\theta}(R_o) = \tau_{rz}(R_o) = 0$, yields the constants of integration $A^{(n)} = B^{(n)} = 0$. In addition, considering stress continuity at laminae interfaces yields $A^{(k)} = B^{(k)} = 0, k = 1 \text{ to } n$. Consequently, $\tau_{r\theta} = \tau_{rz} = 0$ and it holds for all laminae.[15]

Since displacement fields are being sought, the stress components σ_r and σ_θ can be expressed in terms of displacements with the aid of Equation (4.7) thru Equation (4.18). The equilibrium equation, Equation (4.4), thus becomes

$$\frac{\partial^2 u_r^{(k)}}{\partial r^2} + \frac{1}{r}\frac{\partial u_r^{(k)}}{\partial r} - \frac{\overline{C}_{22}^{(k)} \Big/ \overline{C}_{33}^{(k)}}{r^2} u_r^{(k)} = \frac{\overline{C}_{12}^{(k)} - \overline{C}_{13}^{(k)}}{\overline{C}_{33}^{(k)}} \frac{\varepsilon_0}{r} + \frac{\overline{C}_{26}^{(k)} - 2\overline{C}_{36}^{(k)}}{\overline{C}_{33}^{(k)}} \gamma_0 \quad . \tag{4.21}$$

Equation (4.21) is a second-order ordinary differential equation[16] for u_r and can be solved by the Euler Cauchy technique. The complete displacement field solution is explicitly given in Equation (4.22). In Equation (4.22) $D^{(k)}$ and $E^{(k)}$ are constants whose values depend upon the material properties of the laminae. It is noted that the constants ε_0 and γ_0 do not change among laminae.

$$u_r^{(k)} = D^{(k)} r^{\lambda(k)} + E^{(k)} r^{-\lambda(k)} + \alpha_1^{(k)} \varepsilon_0 r + \alpha_2^{(k)} \gamma_0 r^2 , \tag{4.22}$$

where

$$\lambda^{(k)} = \sqrt{\frac{C_{22}^{(k)}}{C_{33}^{(k)}}} , \tag{4.23}$$

$$\alpha_1^{(k)} = \frac{\overline{C}_{12}^{(k)} - \overline{C}_{13}^{(k)}}{\overline{C}_{33}^{(k)} - \overline{C}_{22}^{(k)}} , \tag{4.24}$$

and

$$\alpha_2^{(k)} = \frac{\overline{C}_{26}^{(k)} - 2\overline{C}_{36}^{(k)}}{4\overline{C}_{33}^{(k)} - \overline{C}_{22}^{(k)}}. \tag{4.25}$$

For a composite cylinder with n-plys, ε_0 and γ_0 remain the same for all plys, and there is a different set of D and E for each layer. Overall, a total of $2n+2$ constants is to be determined. The boundary and interfacial conditions needed for solving these unknown constants are listed as follows:[15]

I. Internal and external pressure, P_i and P_0, specified on the inner and outer surfaces:

$$\sigma_r(R_i) = -P_i, \tag{4.26}$$

and

$$\sigma_r(R_o) = P_o = 0 \tag{4.27}$$

II. Radial displacement and radial stress continuity at the laminae interfaces:

$$u_r^{(k)}(r_k) = u_r^{(k+1)}(r_k) \tag{4.28}$$

and

III. Axial load and torque specified at the end of the composite cylinder:

$$2\pi \sum_{k=1}^{n} \int_{r_{k-1}}^{r_k} \sigma_z^{(k)} r dr = F_{applied} + \pi(P_i R_i^2 - P_o R_o^2) \tag{4.29}$$

and

$$2\pi \sum_{k=1}^{n} \int_{r_k}^{r_{k+1}} \tau_{\theta z}^{(k)} r^2 dr = T_{applied}. \tag{4.30}$$

The boundary conditions in Equations (4.29) and (4.30) equate the net force in the axial direction including the end cap effect and applied torque to the cylindrical composite, respectively.[16]

Applying continuity condition for radial displacement and the boundary and interfacial conditions for the corresponding stress components yields a system of $2n+2$ algebraic equations. Equations (4.31) thru (4.35) below are the complete solutions to the axial, circumferential, radial, and in-plane shear stresses for the k^{th} ply, respectively.[17]

$$\sigma_z^{(k)} = (\bar{C}_{12}^{(k)} + \beta^{(k)}\,\bar{C}_{13}^{(k)})D^{(k)}r^{\beta(k)-1} + (\bar{C}_{12}^{(k)} - \beta^{(k)}\,\bar{C}_{13}^{(k)})E^{(k)}r^{-\beta(k)-1} \ldots\ldots, \quad (4.31)$$
$$+ \{\bar{C}_{11}^{(k)} + (\bar{C}_{13}^{(k)} + \bar{C}_{12}^{(k)})\alpha_1^{(k)}\}\varepsilon_0 + \{\bar{C}_{16}^{(k)} + (\bar{C}_{12}^{(k)} + 2\bar{C}_{13}^{(k)})\alpha_2^{(k)}\}\gamma_0 r$$

$$\sigma_\theta^{(k)} = (\bar{C}_{22}^{(k)} + \beta^{(k)}\,\bar{C}_{23}^{(k)})D^{(k)}r^{\beta(k)-1} + (\bar{C}_{22}^{(k)} - \beta^{(k)}\,\bar{C}_{23}^{(k)})E^{(k)}r^{-\beta(k)-1} \ldots\ldots, \quad (4.32)$$
$$+ \{\bar{C}_{12}^{(k)} + (\bar{C}_{22}^{(k)} + \bar{C}_{23}^{(k)})\alpha_1^{(k)}\}\varepsilon_0 + \{\bar{C}_{26}^{(k)} + (\bar{C}_{22}^{(k)} + 2\bar{C}_{23}^{(k)})\alpha_2^{(k)}\}\gamma_0 r$$

$$\sigma_r^{(k)} = (\bar{C}_{23}^{(k)} + \beta^{(k)}\,\bar{C}_{33}^{(k)})D^{(k)}r^{\beta(k)-1} + (\bar{C}_{23}^{(k)} - \beta^{(k)}\,\bar{C}_{33}^{(k)})E^{(k)}r^{-\beta(k)-1} \ldots\ldots, \quad (4.33)$$
$$+ \{\bar{C}_{13}^{(k)} + (\bar{C}_{23}^{(k)} + \bar{C}_{33}^{(k)})\alpha_1^{(k)}\}\varepsilon_0 + \{\bar{C}_{36}^{(k)} + (\bar{C}_{23}^{(k)} + 2\bar{C}_{33}^{(k)})\alpha_2^{(k)}\}\gamma_0 r$$

$$\tau_{z\theta}^{(k)} = (\bar{C}_{26}^{(k)} + \beta^{(k)}\,\bar{C}_{36}^{(k)})D^{(k)}r^{\beta(k)-1} + (\bar{C}_{26}^{(k)} - \beta^{(k)}\,\bar{C}_{36}^{(k)})E^{(k)}r^{-\beta(k)-1} \ldots\ldots \quad (4.34)$$
$$+ \{\bar{C}_{16}^{(k)} + (\bar{C}_{26}^{(k)} + \bar{C}_{36}^{(k)})\alpha_1^{(k)}\}\varepsilon_0 + \{\bar{C}_{66}^{(k)} + (\bar{C}_{26}^{(k)} + 2\bar{C}3_{36}^{(k)})\alpha_2^{(k)}\}\gamma_0 r$$

and

$$\tau_{\theta r}^{(k)} = \tau_{rz}^{(k)} = 0. \quad (4.35)$$

Once the constants are solved, the displacements and stresses are determined.

4.2 Isotropic Layers

Since all COPVs analyzed consist of a titanium liner as schematically shown in Figure 4.2, it is necessary to consider and modify the formulation presented in Section 4.1 for isotropic materials.

Figure 4.2 Titanium Liner

For isotropic materials, there are only two independent material constants, i.e., $C_{11}^{(k)} = C_{22}^{(k)} = C_{33}^{(k)}$, $C_{12}^{(k)} = C_{13}^{(k)} = C_{23}^{(k)}$, and $C_{16}^{(k)} = C_{26}^{(k)} = C_{36}^{(k)} = 0$, and they are related to material mechanical properties as

$$C_{11}^{(k)} = \frac{E(1-v)}{(1-2v)(1+v)}, \tag{4.36}$$

$$C_{12}^{(k)} = \frac{E}{2(1+v)}. \tag{4.37}$$

Similar to the composite cylinder, displacement fields are sought. The stress components σ_r and σ_θ can be expressed in terms of displacements with the aid of Equations (4.7) through (4.18). The general solution of the radial displacement for an isotropic material that satisfies the equilibrium has the following form:

$$u_r^{(k)} = D^{(k)} r + E^{(k)} r^{-1}. \tag{4.38}$$

Applying boundary and interfacial conditions, the complete solutions[17] for the radial displacement, the axial, circumferential, radial, and shear stresses for the isotropic liner can be obtained.[16] Equations (4.39) to (4.43) give the explicit forms of the solutions respectively.

$$\sigma_z^{(k)} = (2\bar{C}_{12}^{(k)})D^{(k)} + \{\bar{C}_{11}^{(k)}\}\varepsilon_0, \tag{4.39}$$

$$\sigma_\theta^{(k)} = (\bar{C}_{11}^{(k)} + \bar{C}_{12}^{(k)})D^{(k)} + (\bar{C}_{11}^{(k)} - \bar{C}_{12}^{(k)})E^{(k)}r^{-2} + \{\bar{C}_{12}^{(k)}\}\varepsilon_0, \tag{4.40}$$

$$\sigma_r^{(k)} = (\bar{C}_{12}^{(k)} + \bar{C}_{11}^{(k)})D^{(k)} + (\bar{C}_{12}^{(k)} - \bar{C}_{11}^{(k)})E^{(k)}r^{-2} + \{\bar{C}_{12}^{(k)}\}\varepsilon_0, \tag{4.41}$$

$$\tau_{\theta r}^{(k)} = \tau_{rz}^{(k)} = 0, \tag{4.42}$$

and

$$\tau_{z\theta}^{(k)} = \{\bar{C}_{12}^{(k)}\}\gamma_0 r. \tag{4.43}$$

4.3 Material Constants

For the orthotropic composite layers, the material modulus matrix elements C were calculated from the engineering constants E, ν and G (Young's moduli, Poisson's ratios, and shear moduli, respectively). Figure 4.3 below illustrates the coordinate system relationship between the principal material axis and the composite cylindrical axis. It highlights that (x, y, z) is the material principal coordinate system where x is the fibers major direction and (r, θ, z) is the composite cylindrical coordinate system.

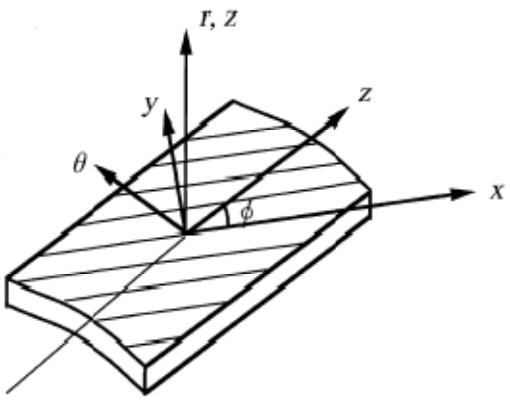

Figure 4.3 Composite Coordinate System[16]

For a unidirectional COPV, the fiber distributions are very similar in the y and z directions. Therefore, assuming transverse isotropy, and based on equivalent properties in the y-z plane for unidirectional material, we get $E_x, E_y, E_z, \nu_{xy}, \nu_{zx}, \nu_{zy}, G_{xx}, G_{yy}, G_{zz}$

where,

$$E_y = E_z, \nu_{xy}, \nu_{zx} = \nu_{zy}, G_{xx}, G_{yy} = G_{zz}$$

and

$$G_{xx} = \frac{E_y}{2(1+\nu_{zy})} \text{ ,} \tag{4.44}$$

where G_{xx} is the transverse shear modulus, E_y is the transverse modulus and ν_{zy} is the transverse Poisson ratio, where x and y refer to material principal axes along fibers and transverse directions, respectively.[16] The conversion of engineering constants to the modulus matrix [16]elements is obtained from Equation (4.45).

$$\begin{bmatrix} C_{xx} & C_{xy} & C_{xz} \\ & C_{yy} & C_{yz} \\ Sym. & & C_{zz} \end{bmatrix} = \begin{bmatrix} 1/E_x & -\nu_{yx}/E_x & -\nu_{yx}/E_x \\ & 1/E_y & -\nu_{zy}/E_y \\ Sym. & & 1/E_z \end{bmatrix}^{-1} . \quad (4.45)$$

The off-axis stiffness constants in Equation (4.47) are calculated from the on-axis stiffness constants by using a stiffness transformation matrix $[A_{kl}]$.[16] Letting (1,2,3) coincide with the (r,θ,z) directions, the compliance matrix in terms of the engineering constants follows:

$$\left\{\overline{C_{ij}^{(k)}}\right\} = [A_{kl}]\left\{C_{ij}^{(k)}\right\}, \quad (4.46)$$

where

$$\left\{\overline{C_{ij}^{(k)}}\right\} = \left\{\overline{C_{11}^{(k)}}, \overline{C_{12}^{(k)}}, \overline{C_{13}^{(k)}}, \overline{C_{16}^{(k)}}, \overline{C_{22}^{(k)}}, \overline{C_{23}^{(k)}}, \overline{C_{26}^{(k)}}, \overline{C_{33}^{(k)}}, \overline{C_{36}^{(k)}}, \overline{C_{44}^{(k)}}, \overline{C_{45}^{(k)}}, \overline{C_{55}^{(k)}}, \overline{C_{66}^{(k)}}\right\}^T \quad (4.47)$$

$$\left\{C_{ij}^{(k)}\right\} = \left\{C_{xx}^{(k)}, C_{yy}^{(k)}, C_{zz}^{(k)}, C_{xy}^{(k)}, C_{xz}^{(k)}, C_{yz}^{(k)}, G_{xx}^{(k)}, G_{yy}^{(k)}, G_{zz}^{(k)}\right\}^T . \quad (4.48)$$

The stiffness transformation matrix[16] for the coordinate system between the on-axis and the cylindrical is given by Equation (4.49) .

$$[A_{kl}]=\begin{bmatrix} m^4 & n^4 & 0 & 2m^2n^2 & 0 & 0 & 0 & 0 & 4m^2n^2 \\ m^2n^2 & m^2n^2 & 0 & m^4+n^4 & 0 & 0 & 0 & 0 & -4m^2n^2 \\ 0 & 0 & 0 & 0 & m^2 & n^2 & 0 & 0 & 0 \\ m^3n & -mn^3 & 0 & -m^3n+mn^3 & 0 & 0 & 0 & 0 & -2m^3n+2mn^3 \\ n^4 & m^4 & 0 & 2m^2n^2 & 0 & 0 & 0 & 0 & 4m^2n^2 \\ 0 & 0 & 0 & 0 & n^2 & m^2 & 0 & 0 & 0 \\ mn^3 & -m^3n & 0 & m^3n-mn^3 & 0 & 0 & 0 & 0 & 2m^3n-2mn^3 \\ 0 & 0 & 1 & 0 & 0 & 0 & 0 & 0 & 0 \\ 0 & 0 & 0 & 0 & mn & -mn & 0 & 0 & 0 \\ 0 & 0 & 0 & 0 & 0 & 0 & m^2 & n^2 & 0 \\ 0 & 0 & 0 & 0 & 0 & 0 & -mn & mn & 0 \\ 0 & 0 & 0 & 0 & 0 & 0 & n^2 & m^2 & 0 \\ m^2n^2 & m^2n^2 & 0 & -2m^2n^2 & 0 & 0 & 0 & 0 & (m^2-n^2)^2 \end{bmatrix}, \quad (4.49)$$

where $m=\cos\phi$ and $n=\sin(\phi)$. Also, the fiber orientation θ is defined as the angle between the fiber direction and the longitudinal axis z of the pressure vessel.

CHAPTER 5

MESSENGER HELIUM COPV CASE STUDY

5.1 Mission

In order to illustrate the application of the proposed nanocomposite hybrid laminae, a case study was performed on the Messenger spacecraft composite over-wrapped helium pressurization tank. The purpose of the Messenger mission is to conduct a scientific investigation of the planet Mercury. The Messenger spacecraft will orbit Mercury after making three flybys of the planet. The spacecraft will enter Mercury orbit in March, 2011, and carry out comprehensive measurements for one full Earth year.[17] Like all spacecrafts that generate thrust by expelling mass, the Messenger spacecraft is governed by Tsiolkovsky's equation. The equation states that if the inert mass of a spacecraft increase the propellant mass increases which will increase the net mass of the spacecraft. The Messenger propulsion system is integrated into the spacecraft structure to make the most economical use of mass.[18] Figure 5.1 is a depiction of the Messenger spacecraft.

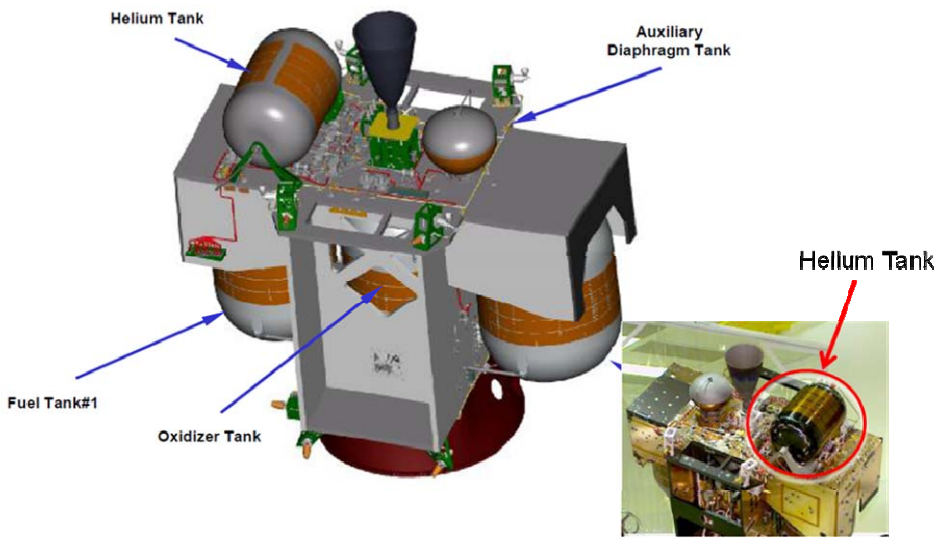

Figure 5.1 Messenger Propulsion System Helium Pressurization Tank[19]

5.1.1 Spacecraft Helium Pressurization Tank

Figure 5.2 below shows the basic configuration of the Messenger Spacecraft filament-wound COPV helium tank. The COPV has a titanium liner that acts as a containment barrier and a overwrap mandrel for the filament winding process.

Figure 5.2 Messenger Helium Tank[19]

The COPV is mounted to the spacecraft using a ported boss fitting and non-ported stinger fitting as seen protruding out of the elliptical domes in Figure 5.2. The ported boss fitting supports the tank in all three directions and incorporates a flat to prevent rotation

about the tank axis. The stinger fitting provides support about the two directions normal to the tank axis while allowing axial growth of the tank during pressurization. The design specifications for the Messenger Spacecraft COPV are shown in Table 5.1.

Table 5.1 Messenger Mechanical Properties

Tank Specifications	Units	Spec
Operating Pressure[19]	MPa	31.026
Total Volume[19]	cubic inches	4040
Max Design Wt.[19]	Lb	23.15
Baseline Wt.[19]	Lb	19.85
Dimensions[19]	Inches	15.8" DIA X 26.25" LONG
Titanium Liner Wall thickness[19]	Inches	0.02
T1000/EPOXY Axial modulus[20]	GPa	165
T1000/EPOXY Transverse Modulus[20]	GPa	7.8
T1000/EPOXY Axial Poisson's ratio[20]	-	0.3
T1000/EPOXY Transverse Poisson's ratio	-	0.52
T1000/EPOXY Axial shear modulus [20]	GPa	4.4
T1000/EPOXY Fiber volume[21]	%	60
T1000/EPOXY density[21]	g/cm^3	1.81
T1000/EPOXY Ultimate Longitudinal Strength[20]	MPa	3040
T1000/EPOXY Ultimate Transverse Strength[20]	MPa	60
T1000/EPOXY In-Plane Shear Strength[20]	MPa	4400
Titanium Density[22]	g/cm^3	4.43
Titanium Tensile Strength, Yield[22]	MPa	880
Titanium Modulus of Elasticity[22]	GPa	113.8
Titanium Poisson's Ratio[22]	-	0.342
Titanium Shear Modulus[22]	GPa	44
Titanium Shear Strength[22]	MPa	550

This case study will determine if the Messenger spacecraft helium pressurization tank mass can be reduced if the PAN-SWCNT/EPOXY nanocomposite is used as the filament overwrap instead of the Toray1000/ EPOXY. This case study will also investigate if reduction in the COPV tank liner thickness can further reduce the overall tank mass.

5.1.2 Filament Winding

To maintain heritage with the messenger tank, the NOPV will have the same filament wound composite structure configuration. However, for analysis purposes, the composite structure is considered to be a laminated cylinder. Figure 5.3 is a graphical illustration of the filament wound process.

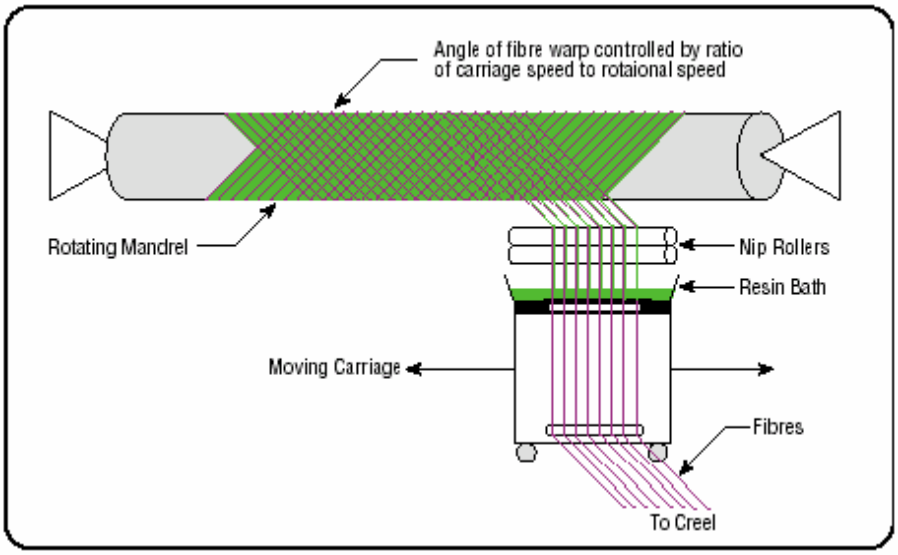

Figure 5.3 Typical Filament Winding Process[23]

During the filament winding process, fibers are attached to a moving carriage and are immersed in a thermosetting resin bath. Next, the carriage translates while the

mandrel rotates. The angle of fiber wrap is controlled by designating the carriage linear speed and the mandrels rotational speed.

CHAPTER 6

RESULTS AND DISCUSSION

6.1 Baseline Tank Comparison

As a practical matter, tanks such as the Messenger Spacecraft Composite Overwrapped Pressure Vessel (MSCOPV) are first made with a very small winding angle, which allows both the cylindrical portion and the end domes to be wrapped simultaneously. Additionally, overlays of hoop wraps on the cylindrical section are needed to resist the hoop stress. To perform the comparison of the T1000/EPOXY and PAN-SWCNT/EPOXY COPV's, a winding angle of 10^0 was selected. The small winding angle was selected since the comparison is based on an alternating angle ply stacking sequence with no hoop wraps. Also, as stated earlier, the angle allows the domes and the cylindrical portion of the tank to be wrapped simultaneously. In the analysis, it was assumed that both tanks are subjected to a uniform internal pressure of 31 MPa. All results are plotted against the non-dimensional radial quantity R defined as[16]

$$R = \frac{r - r_0}{r_a - r_0}, \qquad (6.1)$$

where r is the radial distance and r_0 and r_a are the inner and outer radii, respectively. Also, both tanks are composed of 85 laminae, and strength properties for the T1000\EPOXY are used for all tanks in the analysis.

6.2 Failure Analysis

Failure analysis for the COPV was handled by using two similar failure criteria. For the titanium liner, the Von Misses yield criterion[24] was used. This failure criterion assumes that plastic deformation of the liner begins when the sum of the squares of the principal components of the deviatoric stress reaches the yield strength of the titanium liner.[24] Equation (6.2) represents the equivalent Von Misses stress σ_{mises}^{eq} in the metallic liner.

$$\sigma_{mises}^{eq} = \sqrt{\frac{(\sigma_r - \sigma_\theta)^2 + (\sigma_\theta - \tau_{\theta z})^2 + (\tau_{\theta z} - \sigma_r)^2}{2}} . \tag{6.2}$$

Equation (6.3) listed below illustrates the constraint used in the analysis. It follows that the metallic liner will fail if the equivalent Von Misses stress is greater than the isotropic material yield strength σ_y.

$$\sigma_{mises}^{eq} \leq \sigma_y \tag{6.3}$$

The safety factor of the metallic liner is then calculated based on Equation (6.4). It is defined as the ratio of the isotropic materials yield strength to the equivalent von misses stress

$$SF = \frac{\sigma_y}{\sigma_{mises}^{eq}} . \tag{6.4}$$

Failure in the composite overwrap is addressed by using the Tsai-Hill failure criterion. The Tsai-Hill method is used by treating layers of the composite filament as unidirectional laminae that are considered to be part of the orthotropic laminate. The Tsai-Hill failure theory is based on distortion energy failure theory of von Misses distortional energy yield criterion for isotropic materials as applied to anisotropic materials. Based on the theory, Tsai proposed that a laminae has failed if[12]

$$\left(\frac{\sigma_r}{(\sigma_1^T)_{ult}}\right)^2 - \left(\frac{\sigma_r \sigma_\theta}{(\sigma_1^T)_{ult}}\right) + \left(\frac{\sigma_\theta}{(\sigma_2^T)_{ult}}\right)^2 + \left(\frac{\tau_{z\theta}}{(\tau_{12})_{ult}}\right)^2 < 1, \tag{6.5}$$

where $(\sigma_1^T)_{ult}$ is the composite longitudinal ultimate strength, $(\sigma_2^T)_{ult}$ the composite transverse ultimate strength, and $(\tau_{12})_{ult}$ the in-plane shear ultimate strength.

6.3 NOPV Mass Estimation

The mass of the COPV was calculated by the summation of the mass of the composite layers, the metallic liner and mounting structure. The mass of the metallic liner and composite structure was calculated by computing the volume of each component and then multiplying it by its density, while the mounting structure mass is assumed to be that of the hardware used on the Messenger Spacecraft. The volume of the composite overwrap and metallic liner portion was calculated by separating the tank into two geometric forms. The barrel section of the tank was idealized as a hollow cylinder and the two ellipsoidal end caps were treated as hollow ellipsoids. Equation (6.6) below was used to calculate the total volume for the metallic liner and composite filament portions of the COPV.

$$Vol_{liner,filament} = VolH_{ellipsoid} + Vol_{cylinder}\ . \tag{6.6}$$

In Equation (6.6) $Vol_{liner,filament}$ is the volume of the composite and metallic liner, $VolH_{ellipsoid}$ the volume of the ellipsoidal end cap, and $Vol_{cylinder}$ the volume of the cylindrical section of the tank. The volume of the ellipsoidal end cap is calculated below by

$$VolH_{ellipsoid} = \frac{4}{3}\pi\left(a_e b_e c_e - a_i b_i c_i\right), \tag{6.7}$$

where, a_e, b_e, c_e, are the major, minor, and vertical-axes of the external ellipsoid and a_i, b_i, c_i, are the major, minor, and vertical-axes of the internal ellipsoid, respectively. The volume of the barrel section $Vol_{cylinder}$ is determined by

$$Vol_{cykinder} = \pi(r_o^2 - r_i^2)l_{cyl}, \tag{6.8}$$

where r_o is the outer radius of the cylindrical section, r_i the inner radius of the cylindrical section, and l_{cyl} the length of the cylindrical section. The total mass of the composite overwrapped pressure vessel is then calculated by

$$mass_{COPV} = mass_{liner} + mass_{filament} + \psi, \tag{6.9}$$

where the mass of the composite and metallic liner are represented below in Equation (6.10) and (6.11).

$$mass_{liner} = \rho_{Ti}\left(VolH_{ellipsoid} + Vol_{cykinder}\right), \tag{6.10}$$

$$mass_{filament} = \rho_c\left(VolH_{ellipsoid} + Vol_{cykinder}\right), \tag{6.11}$$

where ρ_{Ti} and ρ_c is the density of the density of Titanium liner and the composite filament respectively. ψ in Equation (6.9) is a constant that represents the sum of the masses for the additional materials and mounting structure for the Messenger Spacecraft.

These masses include the ported boss and stinger on the elliptical dome caps and the film adhesive applied to the liner.

6.4 Baseline Comparison Results

The radial strain distrubtion is shown in Figure 6.1. The plot reveals that the radial strain is compressive and has a linear distribution through the non-dimensional wall thickness of both COPV's. Figure 6.1 also highlights that under the same internal pressure the T1000/EPOXY COPV has larger radial strains induced than the PAN-SWCNT/EPOXY COPV. Additionally, Figure 6.1 shows the discontinuity at the interface of the liner and composite overwrap in both tanks. Also from Figure 6.1 it can be seen that the PAN-SWCNT/EPOXY COPV experienced more deformation in the radial direction.

The constant tensile strain in axial direction through the non-dimensional wall thickness of both COPV's is illustrated in Figure 6.2. It can be seen that the T1000/EPOXY COPV experienced the lager axial strain. For the stacking sequence used, this increase in axial strain is attributed to T1000/EPOXY COPV possessing a larger stiffness in the hoop direction than the PAN-SWCNT/EPOXY COPV and relatively small stiffness in the axial direction.

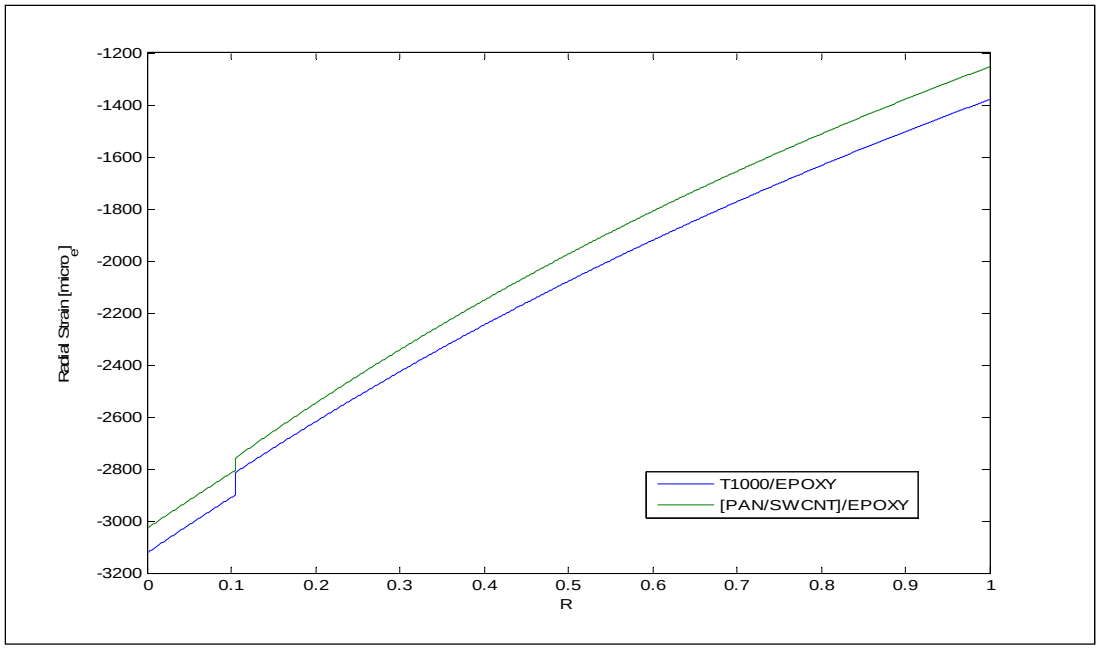

Figure 6.1 Baseline Radial Strain vs. Non-Dimensional Radial Distance

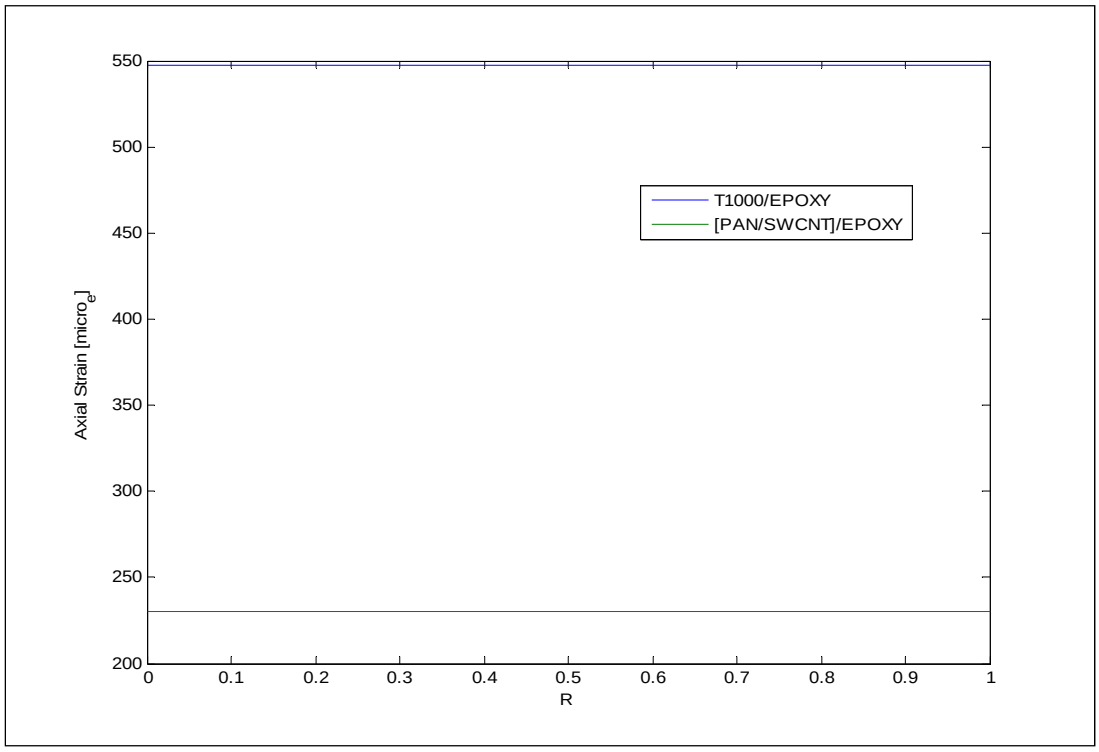

Figure 6.2 Baseline Axial Strain vs. Non-Dimensional Radial Distance

The tensile strain in the circumferential direction through the non-dimensional wall thickness is shown in Figure 6.3. The figure highlights that the circumferential strain distributions are comparable for both COPV's. However, it can be seen that the PAN-SWCNT/EPOXY COPV exhibited greater strains in the circumferential direction than the T1000/EPOXY COPV. This increase in circumferential strain is attributed to the T1000/EPOXY COPV possessing higher stiffness in the hoop direction than the PAN-SWCNT/EPOXY COPV. Moreover, the increase can be explained by Equation (4.13) which relates hoop strain to radial displacement and radial distance. Therefore, the PAN-SWCNT/EPOXY COPV possessed larger circumferential strains since it experienced the most radial deformation.

The compressive shear strain distribution through the nondimensional wall thickness of the COPV's analyzed is shown in Figure 6.4. The figure clearly shows the discontinuity at the interface of the liner and the composite overwrap for both COPV's. Also, it highlights that the PAN-SWCNT/EPOXY COPV experiences slightly larger shear strains than the T1000/EPOXY COPV. This increase in shear strain is attributed to the PAN-SWCNT/EPOXY COPV possessing a larger twist-rate γ_0 than the T1000/EPOXY COPV.

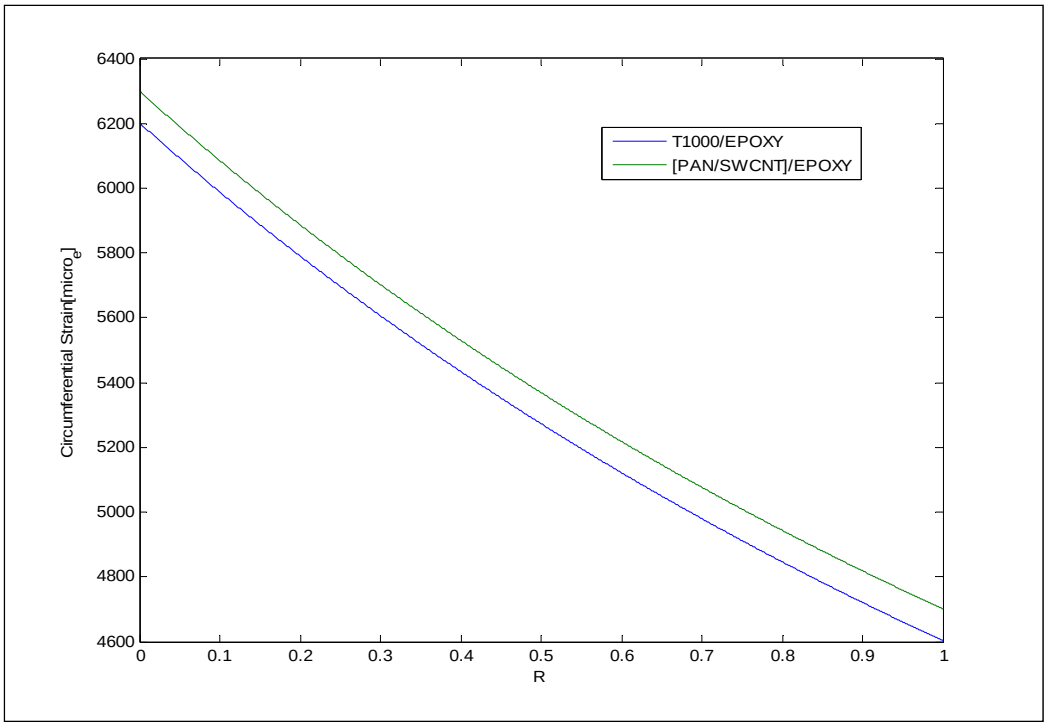

Figure 6.3 Baseline Circumferential Strain vs. Non-Dimensional Radial Distance

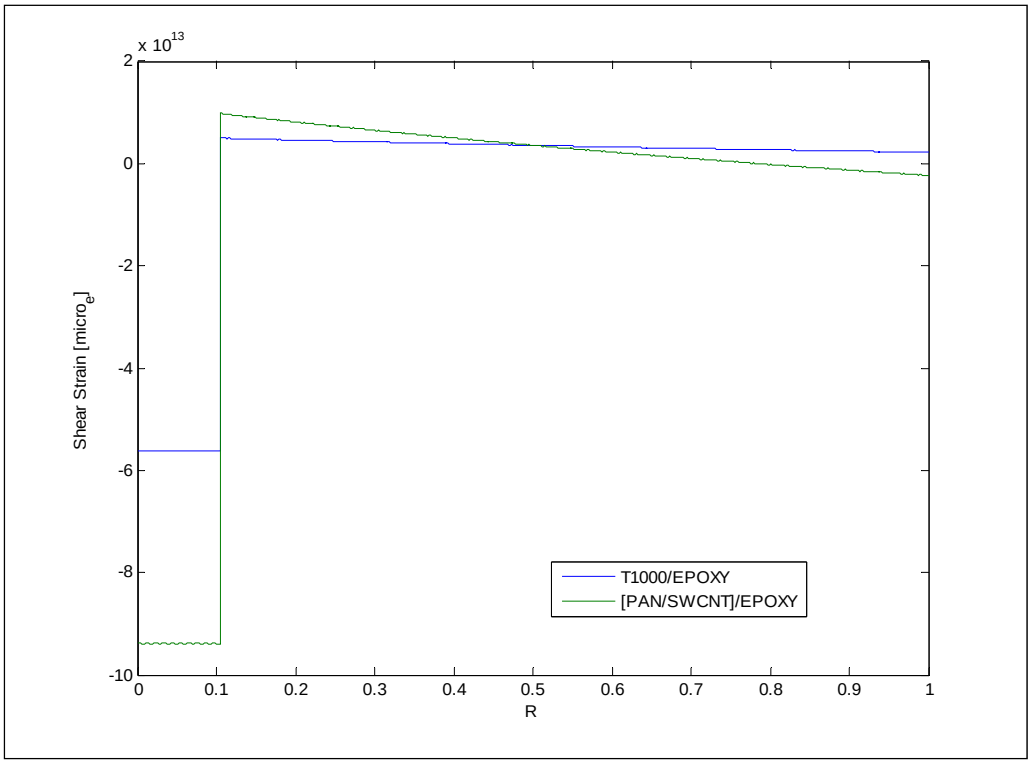

Figure 6.4 Baseline Shear Strain vs. Non-Dimensional Radial Distance

The compressive radial stress distribution through the non-dimensional wall thickness for both COPV's analyzed is plotted in Figure 6.5. The figure illustrates the discontinuity at the interface of the liner and the composite overwrap in both tanks. Also, the figure highlights that the radial stress distributions within the layers possess nearly linear variations. Moreover, the figure indicates that the stresses in the radial direction for both COPV's are comparable.

The tensile circumferential stress distribution through the non-dimensional wall thickness for both COPV's analyzed is plotted in Figure 6.6. For each COPV analyzed the greatest circumferential stress occurred in the isotropic titanium liner. This increase in axial stress stems from the orthotropic composite material exhibiting greater stiffness in the hoop direction than the titanium liner. Additionally, the figure clearly indicates that there is almost no difference in the hoop stress distributions for the composite laminates in both tanks.

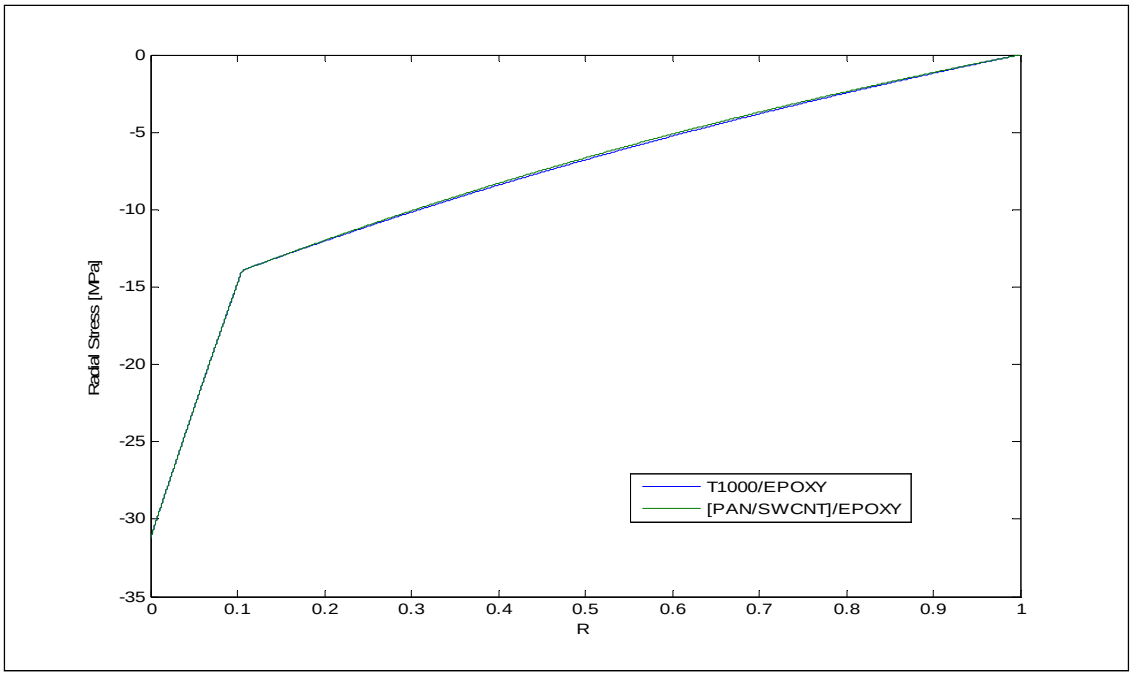

Figure 6.5 Baseline Radial Stress vs. Non-Dimensional Radial Distance

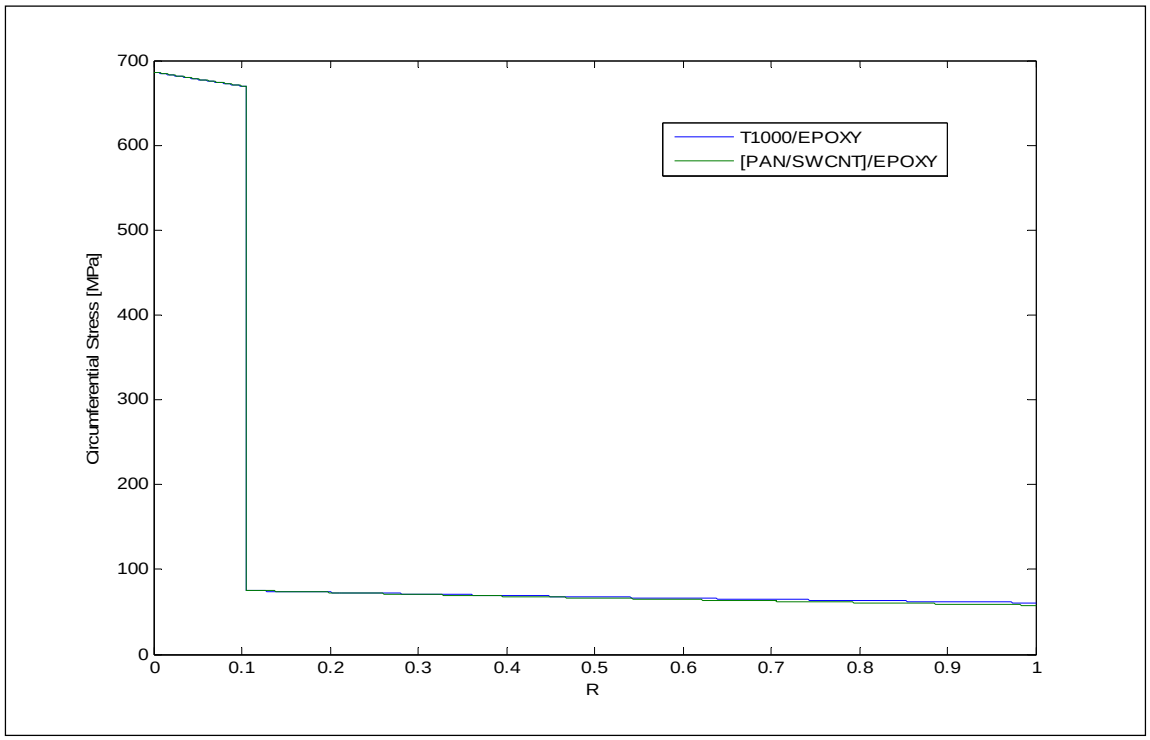

Figure 6.6 Baseline Circumferential Stress vs. Non-Dimensional Radial Distance

The tensile axial stress distribution through the non-dimensional wall thickness for both COPV's analyzed is plotted in Figure 6.7. For both COPV's, the greatest axial stress occurred in the isotropic titanium liner. This increase in axial stress stems from the orthotropic composite material exhibiting greater stiffness in the axial direction than the titanium liner. Furthermore, the figure clearly indicates that there is almost no difference in the hoop stress distributions as well for the composite laminates in the both tanks

The shear stress distributions through the non-dimensional wall thickness for both COPV's analyzed are plotted in Figure 6.8. From Figure 6.8, it can be seen that the PAN-SWCNT/EPOXY COPV experienced the larger shear stress. For the stacking sequence used, this increase in the shear stress is attributed to the PAN-SWCNT/EPOXY COPV possessing a larger γ_0 than the T1000/EPOXY COPV.

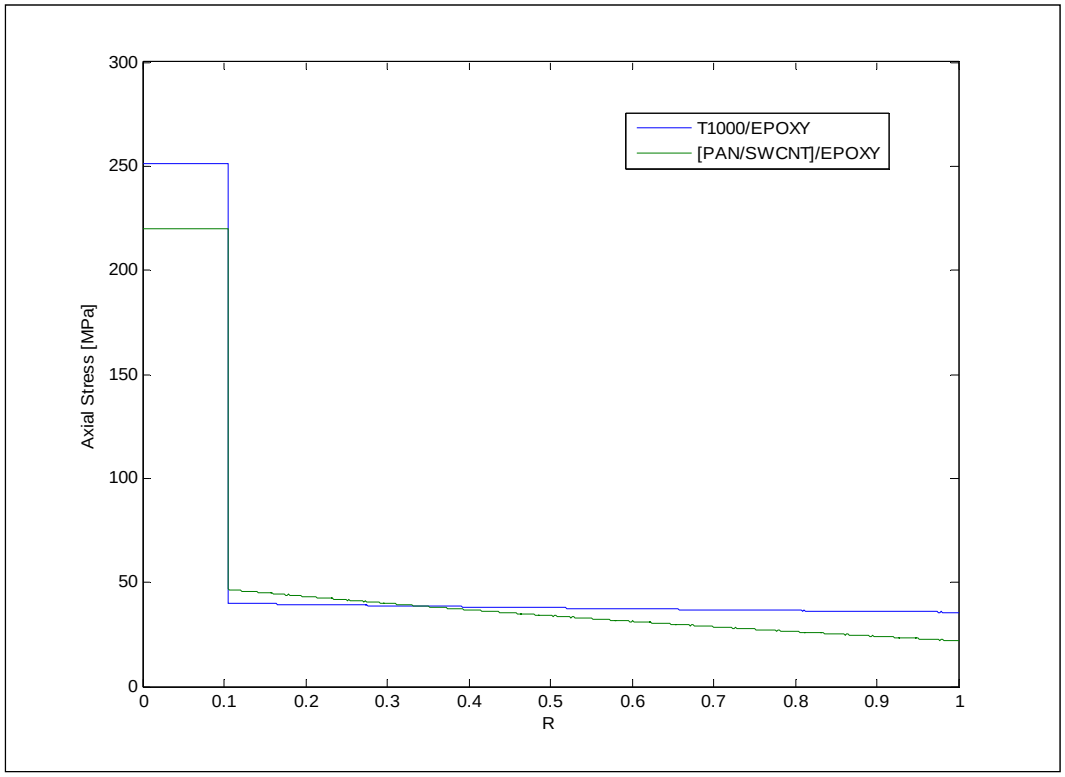

Figure 6.7 Baseline Axial Stress vs. Non-Dimensional Radial Distance

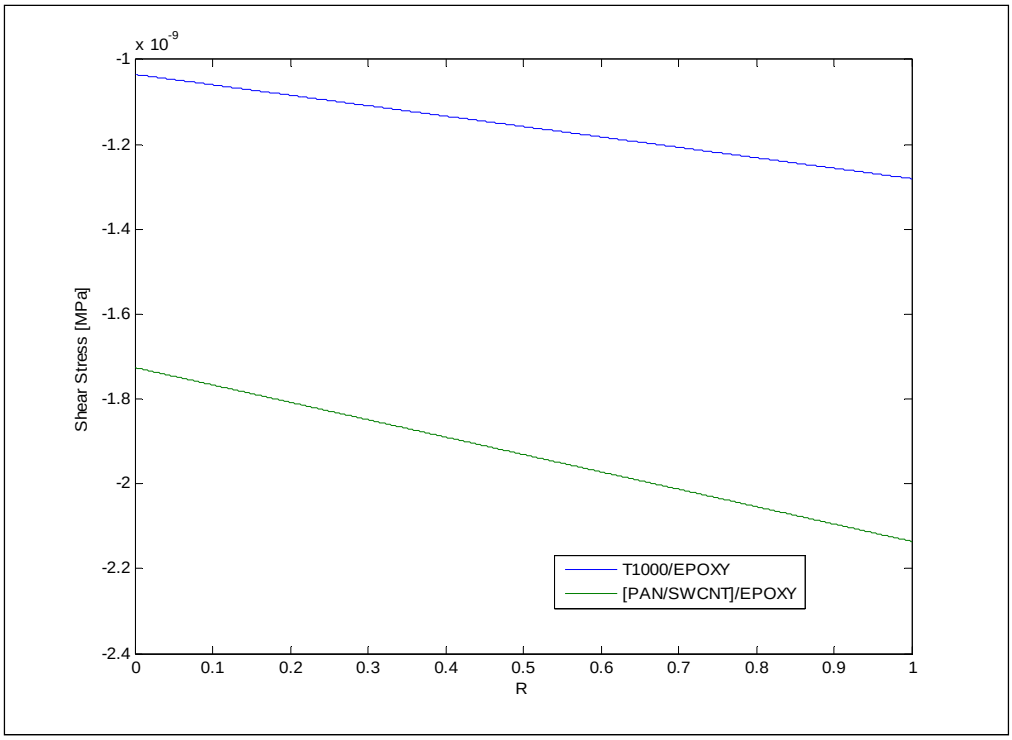

Figure 6.8 Baseline Shear Stress vs. Non-Dimensional Radial Distance

The radial displacement distribution through the non-dimensional wall thickness for both COPV's analyzed is shown in Figure 6.9. The figure indicates that the PAN-SWCNT/EPOXY COPV exhibits greater radial displacement than the T1000/EPOXY COPV. This difference in radail diplacement could result from the greater material anisotropy in the PAN-SWCNT/EPOXY COPV when compared to the T1000/EPOXY COPV.

The constant twist rate γ_0 for each COPV analyzed through the non-dimensional wall thickness is shown in Figure 6.10. The figure reveals that the PAN-SWCNT/EPOXY COPV exhibits the larger twist rate. This increase in γ_0 could be due to higher material anisotropy in the PAN-SWCNT/EPOXY COPV when compared to the T1000/EPOXY COPV.

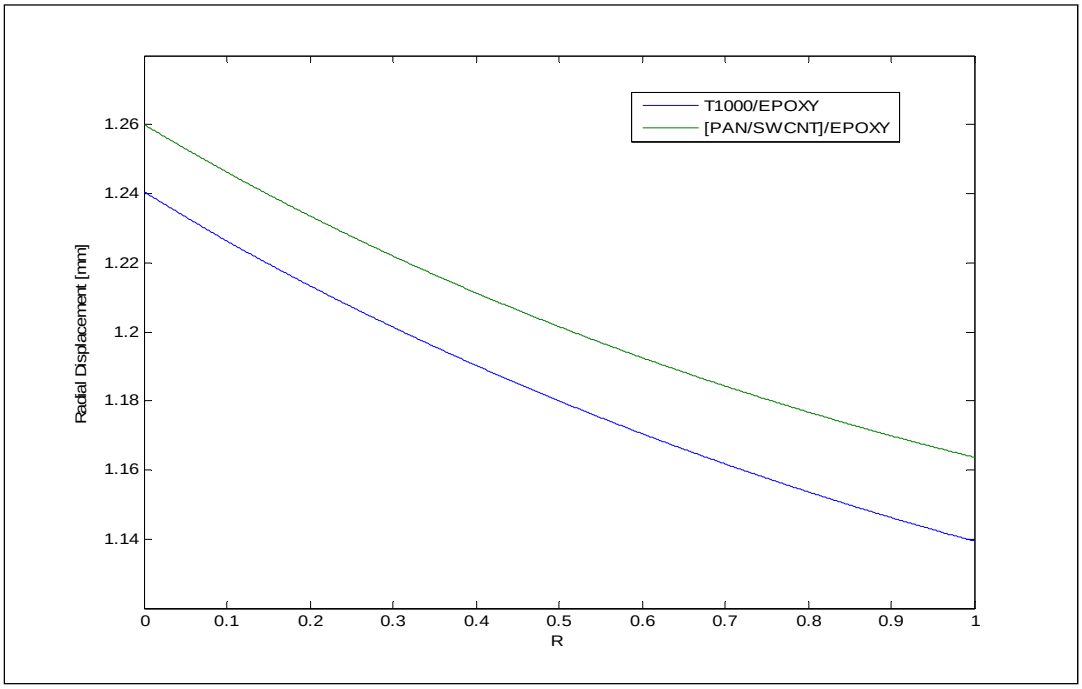

Figure 6.9 Baseline Radial Displacement vs. Non-Dimensional Radial Distance

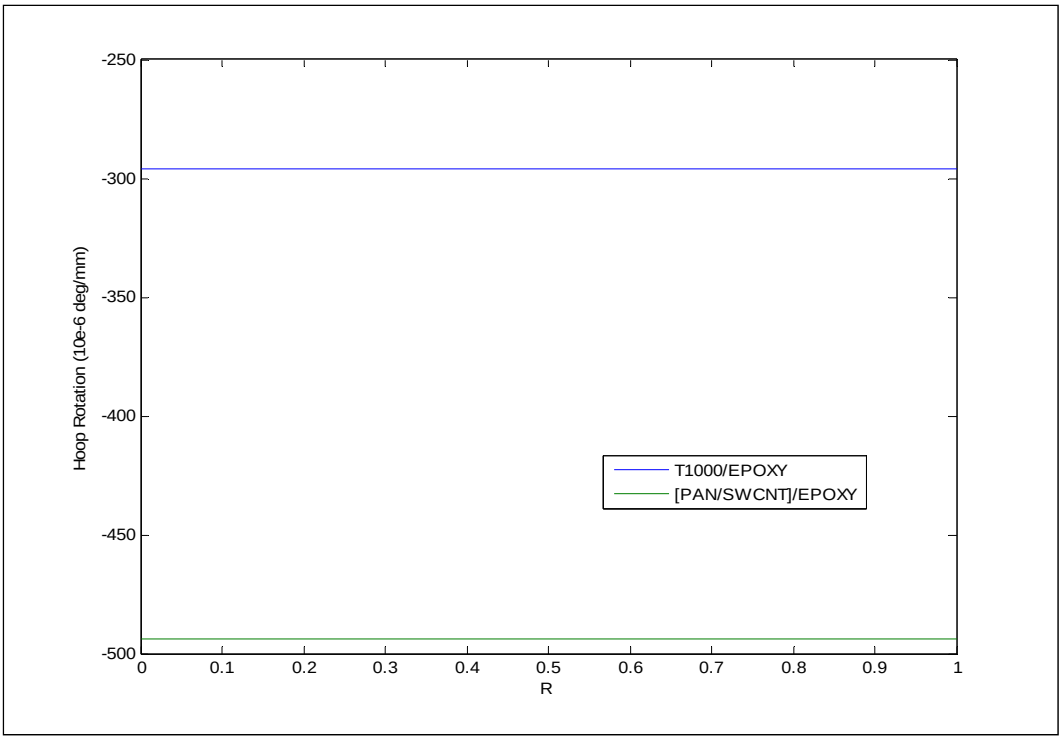

Figure 6.10 Baseline Hoop Rotation vs. Non-Dimensional Radial Distance

In addition to plotting the stress distributions through the COPV thickness, a failure analysis was performed on the metallic liner and composite overwrap. The maximum radial, circumferential, axial, and shear stresses in the metallic liner and composite overwrap layers were used for Equations (6.2), (6.4) and (6.5) to calculate the von Mises stress in the liner, the factor of safety and the Tsai-Hill number for the composite overwrap respectively.

The MATLAB code was used to analyze the metallic liner for each COPV. Ten isotropic layers were assigned to represent the total thickness of the metallic liner. As a result, the Laminae 0 identifier was designated for the isotropic metallic linear layers. The results on the metallic liner failure analysis are shown in Table 6.1. Table 6.1 contains a truncated list of von Mises stresses computed in the metallic liner and shows only five of the ten isotropic layers for the Titanium liner for the T1000/EPOXY and PAN-SWCNT/EPOXY pressure vessels. It can be seen that the differences in the von Mises stress in the liner for each COPV was negligible. It also shows that the liner has a sufficiently high Factor of Safety under the applied loading, since a factor of safety of 1.25 is recommended for aerospace applications.[24]

Table 6.1 Baseline Liner Failure Results

	[Toray 1000/Epoxy]			PAN-SWCNT/EPOXY		
Laminae	STATUS	Von Mises [MPa]	FS	STATUS	Von Mises [MPa]	FS
laminae 0	PASS	671.3	1.3	PASS	671.5	1.3
laminae 0	PASS	670.3	1.3	PASS	670.6	1.3
laminae 0	PASS	669.4	1.3	PASS	669.6	1.3
laminae 0	PASS	668.5	1.3	PASS	668.7	1.3

There was a total of eighty-five composite laminae analyzed for each COPV. The Tsai-Hill number calculated for ten of the eighty-five composite laminae is shown in Table 6.2. The results show that the maximum Tsai-Hill number for each lamina did not exceed the established failure criteria of one.

Table 6.2 Baseline Filament Failure Results

	[Toray 1000/Epoxy]		PAN-SWCNT/EPOXY	
Laminae	STATUS	TSAI-HILL	STATUS	TSAI-HILL
laminae 1	PASS	0.88	PASS	0.89
laminae 2	PASS	0.87	PASS	0.88
laminae 3	PASS	0.87	PASS	0.87
laminae 4	PASS	0.86	PASS	0.87
laminae 5	PASS	0.86	PASS	0.86
laminae 6	PASS	0.85	PASS	0.86
laminae 7	PASS	0.85	PASS	0.85
laminae 8	PASS	0.84	PASS	0.84
laminae 9	PASS	0.84	PASS	0.84
laminae 10	PASS	0.83	PASS	0.83

The results in the comparison of baseline COPV analysis show that each COPV passes failure criteria established for the metallic liner and the composite filament. Though the magnitudes in stress distributions were different in the COPV's, the results in the failure analysis for both COPV's were comparable. The similarities in the results of failure analysis can be attributed to the similarities in material properties.

CHAPTER 7

PARAMETRIC STUDIES

The focus of the tank design was mainly to minimize the mass of the pressure vessel. As a result, parametric studies were performed. To minimize mass, an ultra-thin metallic liner overwrapped with a high strength carbon/epoxy composite was selected as the baseline design. The key design consideration for the NOPV is the maximum expected operating internal pressure. The Toray T1000/Epoxy composite strength properties were used as the strength of the PAN-SWCNT/EPOXY due to the lack of available data. Strength properties of Ti-3Al-2.5V were used for the COPV and NOPV titanium liner. In the parametric analysis of the NOPV, the PAN-SWCNT/EPOXY properties listed in Table 3.1 were used. In addition to the ply properties, the thickness of each ply was limited to .05 mm for all the analyses.

7.1 Fiber Orientation Optimization

Analysis for optimal fiber orientation was performed by evaluating a NOPV subjected to a uniform internal pressure of 31 MPa. The tank geometry was restrained to match that of the Messenger Spacecraft Composite Overwrap Pressure Vessel (MSCPOV). The composite overwrap has a total of 95 plies and the liner has a thickness of .02", which was modeled as ten isotropic layers. The analysis varied the orientation of

the alternating angle ply stacking sequence of the composite overwrap. The fiber orientation ranged from 10^0 too 80^0. The term optimal-fiber orientation is taken to mean the minimal angle needed to sustain the given internal pressure by the filament and liner without failure based on the criterion given in Equation (7.1).

$$f_\theta(\theta) = \begin{cases} pass \quad if \quad \max(Tsai_{Hill}) < 1 \quad and \quad \min(Safety_{Factor}) \geq 1.25 \\ fail \quad if \quad \max(Tsai_{Hill}) > 1 \quad and \quad \min(Safety_{Factor}) \leq 1.25 \end{cases}. \tag{7.1}$$

where $f_\theta(\theta)$ is a piecewise function that outputs pass or fail based on the failure criteria results of the helical winding angle θ specified. The MATLAB Subroutine for Equation (7.1) can be found in Appendix C. The fiber orientation θ is defined as the angle between the fiber direction and the laminates longitudinal axis. In the computation, $f_\theta(\theta)$ takes the maximum Tsai-Hill value for each layer and the maximum Safety Factor in the titanium liner and compares them to 1 and 1.25 respectively. The Safety Factor of 1.25 was used because it is the recommended value for aerospace applications.[24]

Figure 7.1 shows the NOPV maximum Tsai-Hill value and liner SF versus helical winding angle.

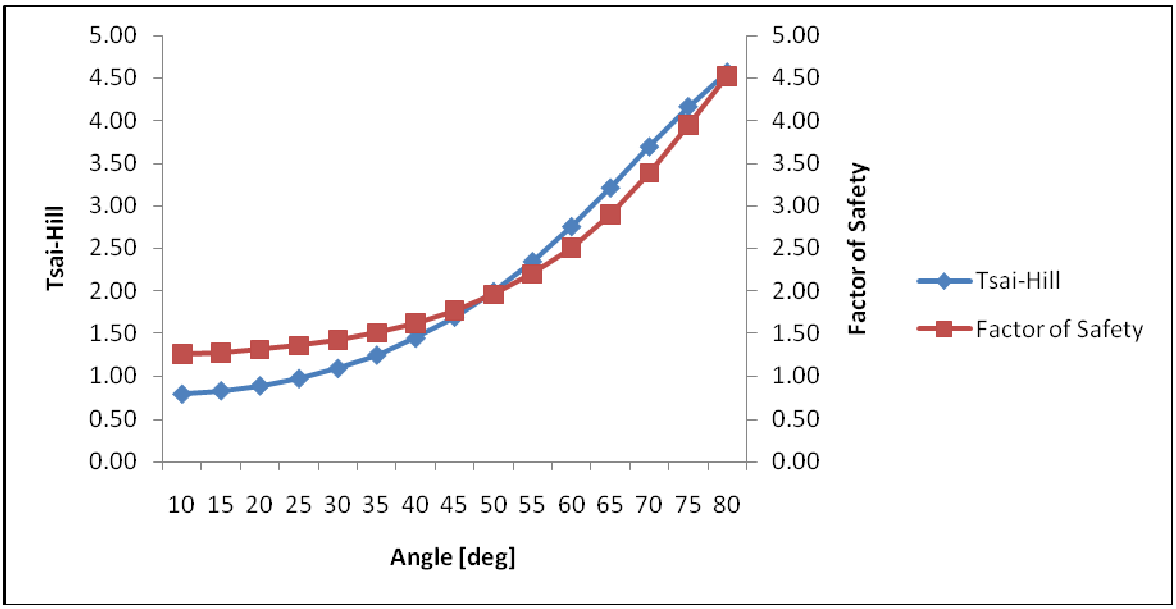

Figure 7.1 Tsai-Hill and Liner SF vs. Helical Winding Angle

From Figure 7.1, it can be seen that the optimal fiber orientation, i.e., the optimum helical winding angle, is 20^0, since it satisfies the constraints established in Equation (7.1). The relatively small winding angle results from the high stresses exhibited in the NOPV axial direction.

7.2 Liner Thickness Optimization

To further improve the weight performance of the NOPV, an analysis for optimal metallic liner thickness was performed. This analysis is performed by reducing the thickness of the liner and increasing the thickness of the composite over-wrap. Though the liner thickness will undergo reduction, care is taken to not sacrifice strength in the NOPV. In the analysis, the inner radius of the NOPV remained .2 m. The 20^0 optimal fiber orientation determined in Section 7.1 was used. The range of the titanium liner thickness was from .012", one half of the thickness of the baseline NOPV, to .02". For each liner thickness, the total number of helical layers was obtained such that the failure

criterion is satisfied in each individual laminae, and the required factor of safety is also achieved on the titanium liner. Equation (7.2) below is the failure criterion used for the analysis of the optimal thickness of the titanium liner.

$$f_N(N) = \begin{cases} pass \quad if \quad \max(Tsai_{Hill}) < 1 \quad and \quad \min(Safety_{Factor}) \geq 1.25 \\ fail \quad if \quad \max(Tsai_{Hill}) > 1 \quad and \quad \min(Safety_{Factor}) \leq 1.25 \end{cases}. \tag{7.2}$$

Though Equation (7.2) shows some resemblance to Equation (7.1), it is a failure function $f_N(N)$ that uses the number of layers N as an independent variable. The MATLAB Subroutine for Equation (7.2) can be found in Appendix D. The variable N is the number of layers the composite overwrap needed to maintain a Tsai-Hill and SF less than 1 and greater than 1.25 for the composite and titanium liner respectively.

7.2.1 Liner Thickness Optimization Results

Figure 7.2 through Figure 7.6 are plots that show the Tsai-Hill and liner-safety factor versus total number of layers. For each case, the number of composite layers needed to support the applied internal pressure can be seen graphically.

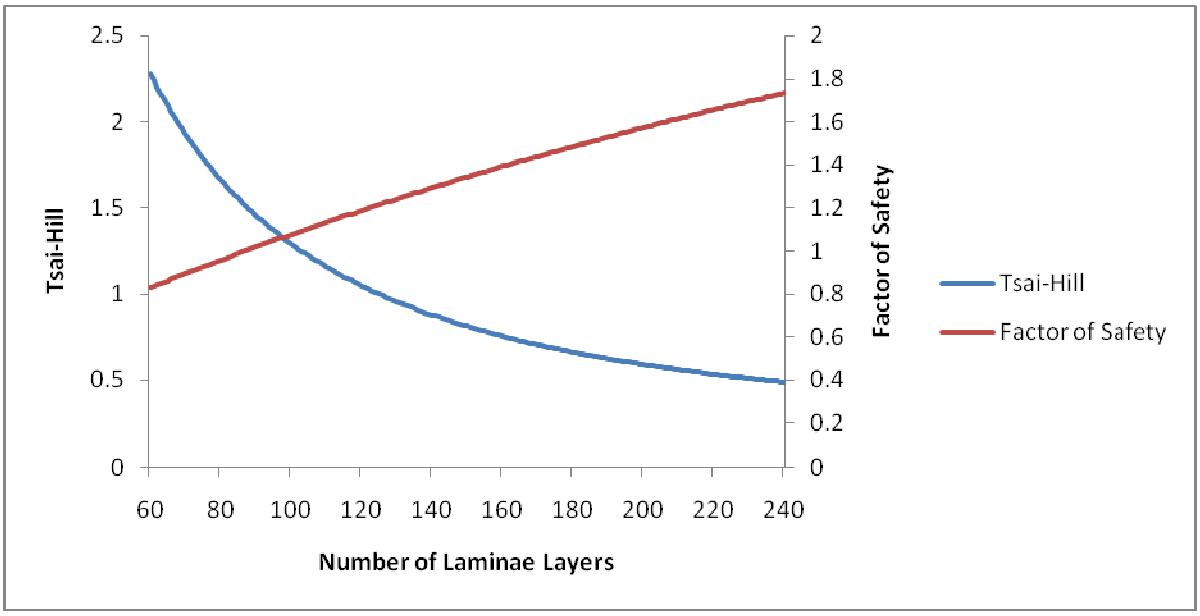

Figure 7.2 Tsai-Hill and Liner SF vs. Number of Layers for CASE 1

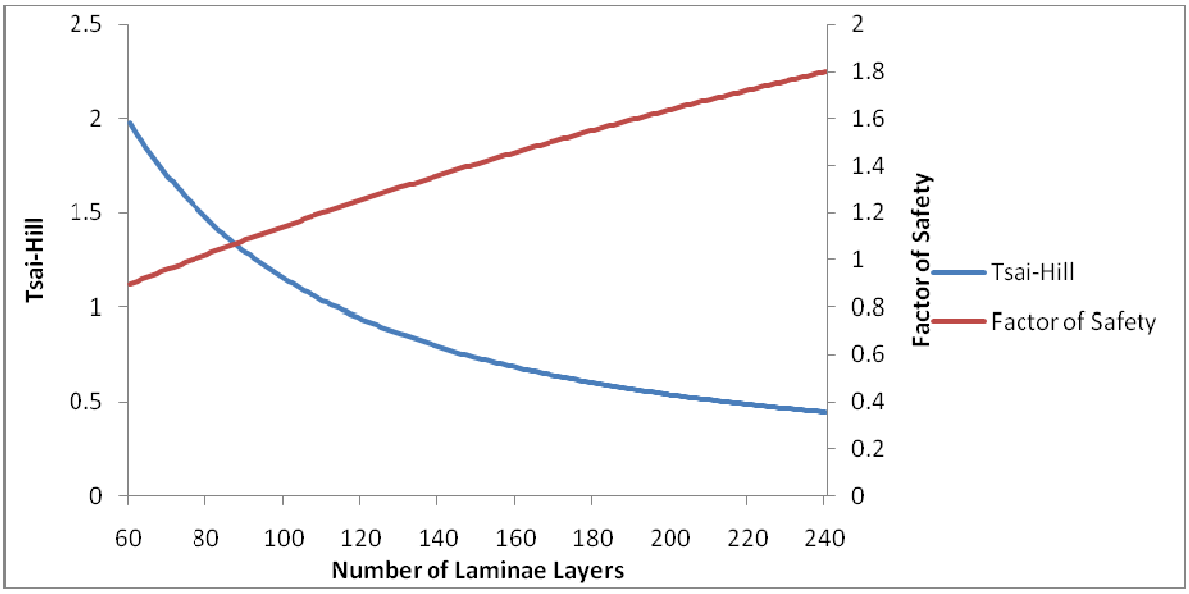

Figure 7.3 Tsai-Hill and Liner SF vs. Number of Layers for CASE 2

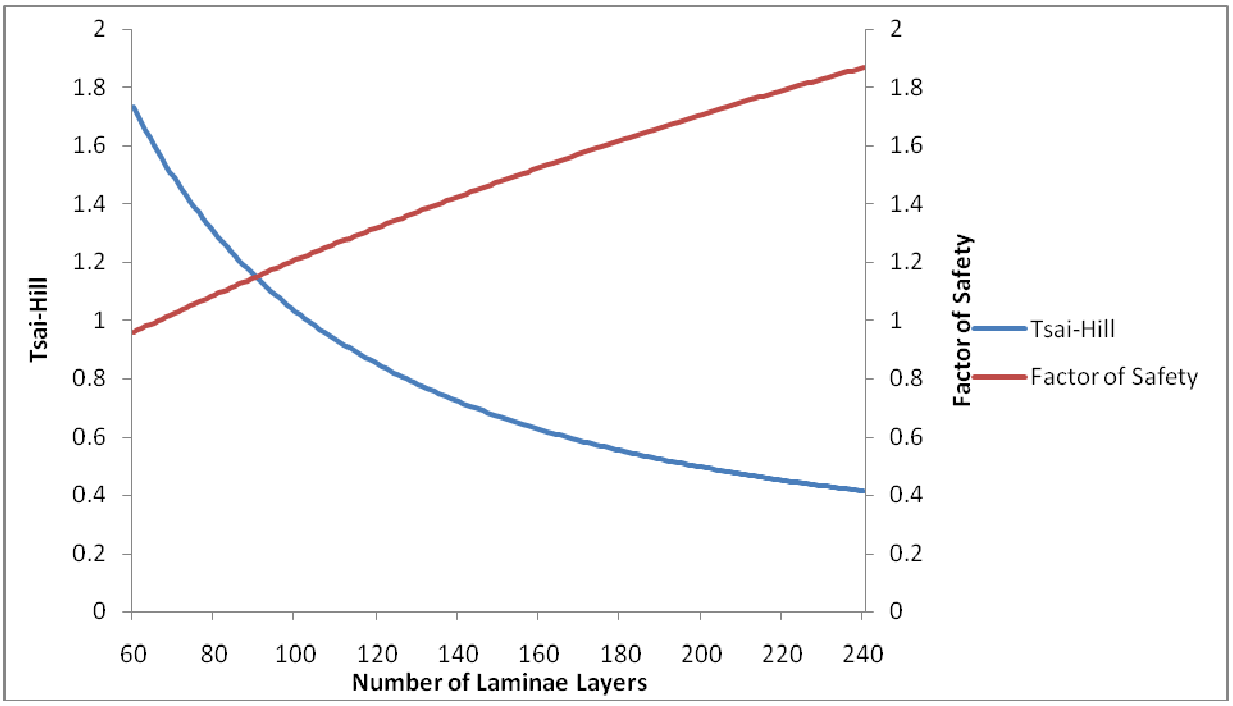

Figure 7.4 Tsai-Hill and Liner SF vs. Number of Layers for CASE 3

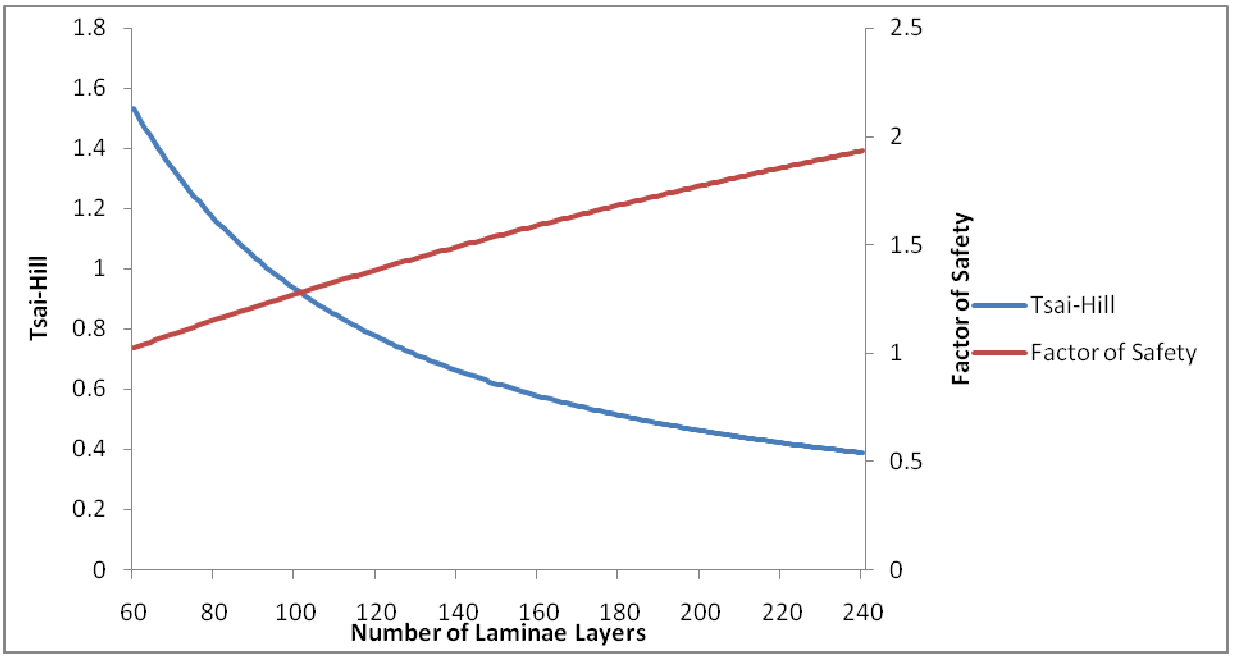

Figure 7.5 Tsai-Hill and Liner SF vs. Number of Layers for CASE 4

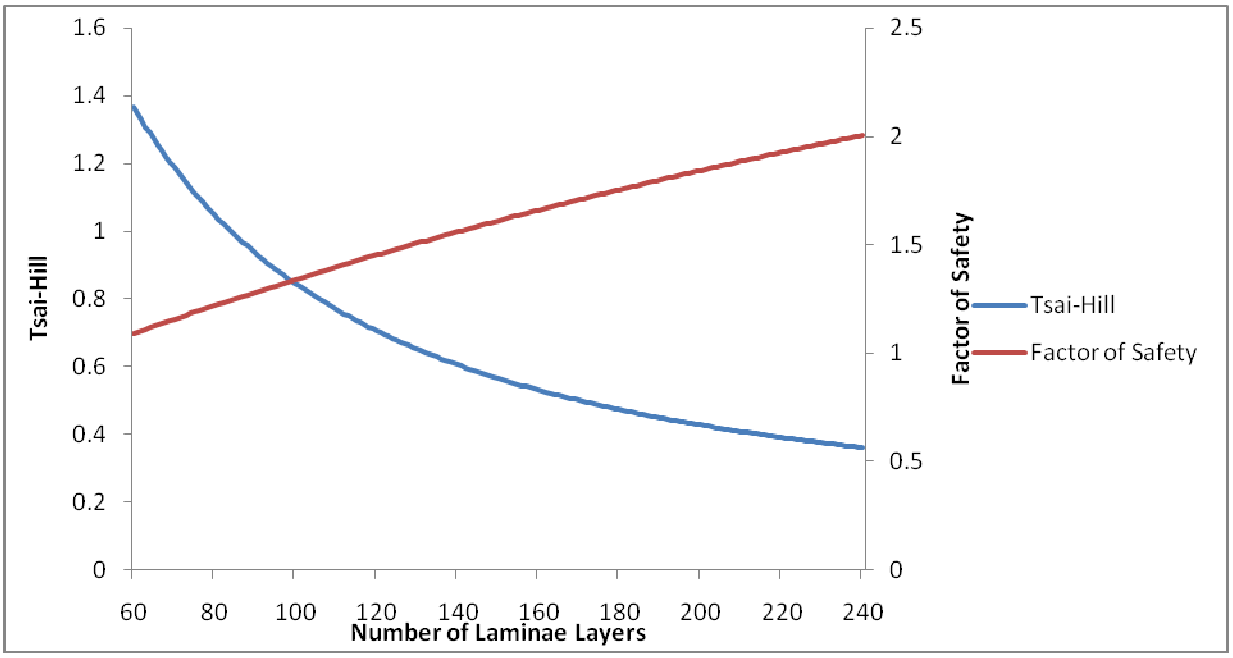

Figure 7.6 Tsai-Hill and Liner SF vs. Number of Layers for CASE 5

From Figure 7.2 to Figure 29, it can be seen that as the liner thickness decreased the number of the composite layers increased in order to satisfy the COPV failure criterion. Table 7.1 below displays the number of composite layers needed for each case analyzed.

Table 7.1 Composite Layers Needed

CASE	Liner Thickness [inches]	Composite layers
1	0.012	127
2	0.014	113
3	0.016	99
4	0.018	87
5	0.02	75

To evaluate the overall mass impact, the tank weight was calculated for Cases 1 through 5. Figure 7.7 is a bar chart that shows the computed mass of the five cases analyzed. Each case was compared with the overall baseline tank mass for the T1000/EPOXY and the NOPV, which were 19.85 lb and 16.94 lb, respectively.

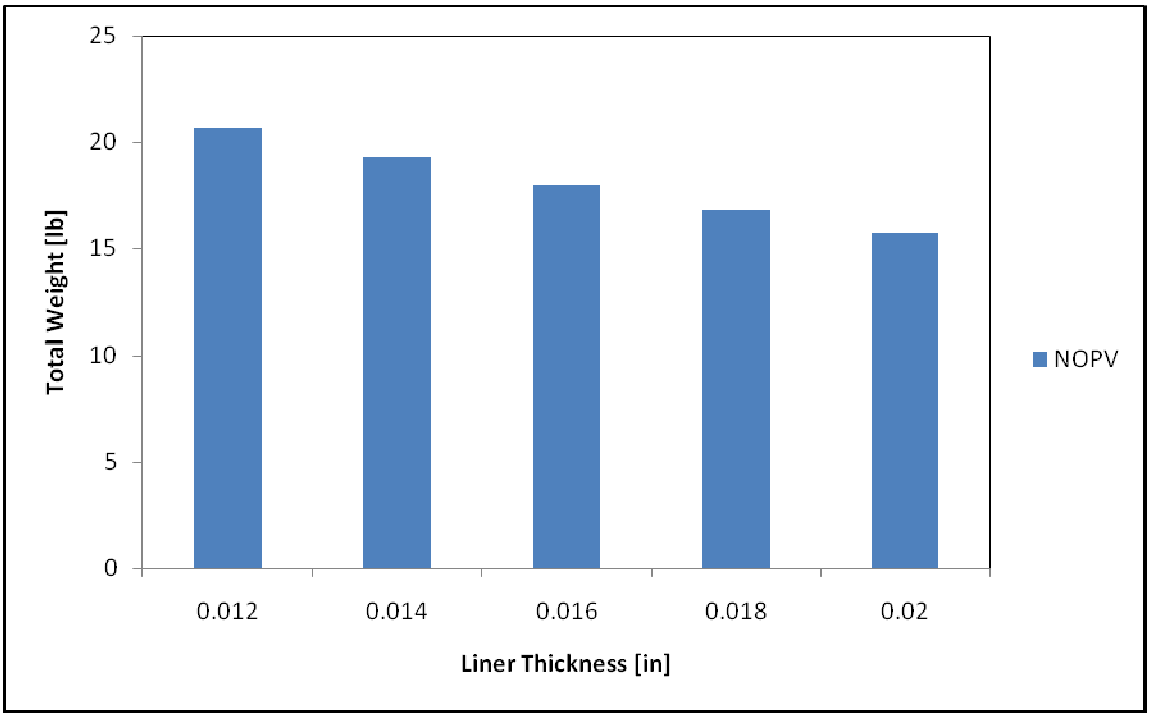

Figure 7.7 NOPV weight vs. Titanium Liner Thickness

It is apparent that as the liner thickness decreases, the overall NOPV structural mass increases. This trend can be explained by the increase in the composite layers needed to sustain a reduction in the titanium liner's thickness. From Table 7.1, it can be seen that Case 1, which had a liner thickness of .012," required 127 composite layers, whereas a liner thickness of .02" required only 75 layers. The additional composite layers negated any weight reductions obtained from decreasing the liner thickness.

To better understand the mass impact with regard to liner thickness reduction the difference in weight when compared to the two baseline tank weights is plotted in Figure 7.8.

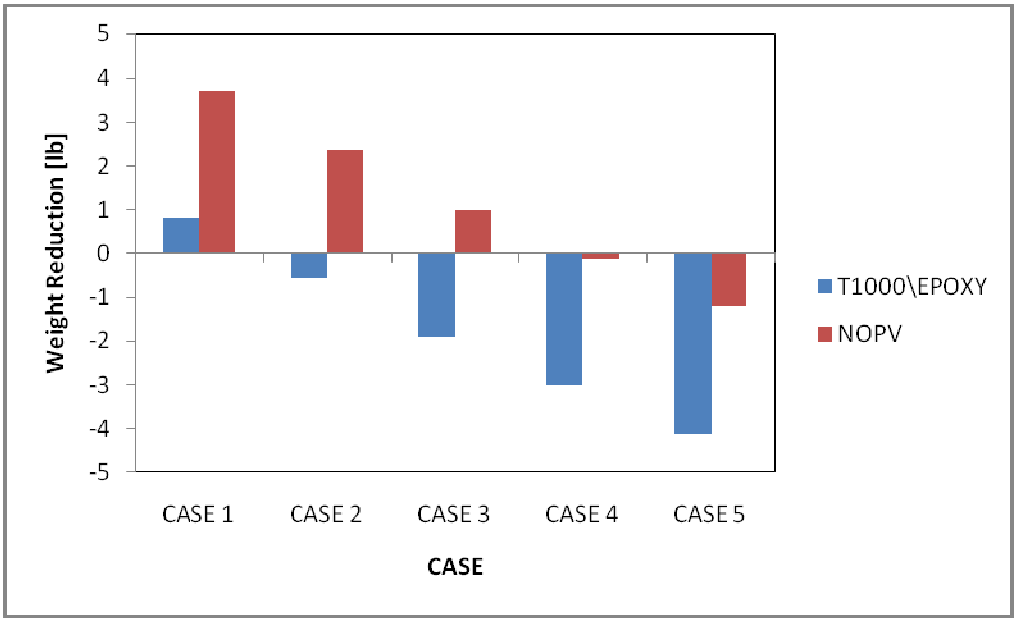

Figure 7.8 NOPV Weight Reduction Comparison

In Figure 7.8, positive and negative weight values are used to represent an increase or decrease in weight respectively. It illustrates that for Cases 1 through 3, the NOPV weight was greater than the NOPV baseline tank weight. The increase in the weight ranged from 3.7 to 0.9 lbs for the first 3 cases. Also, the NOPV weight was larger than the baseline T1000\EPOXY tank in Case 1. However, this increase in weight was not true for Cases 2 through 5, where the NOPV weighed less than the baseline T1000\EPOXY tank. For Cases 2 through 5, the weight reduction ranged from 0.6 to 4.1 lbs with respect to the baseline T1000\EPOXY tank. Furthermore, for Cases 4 and 5 the NOPV weighed less than the baseline NOPV tank with the maximum weight saving of 1.2 lb in Case 5.

The results of the case study for liner thickness reveal that the optimum liner thickness is .02". Also, they suggest that the weight performance of the tank decreases as the liner thickness decreases. This reduction in weight performance is caused by the increase in composite layers on the NOPV required to sustain the applied internal pressure of 31 MPa.

In summary, the parametric studies yielded an optimal winding angle and liner thickness of 20^0 and .02". Since weight reduction is a primary design goal, it is clear that the winding angle and liner thickness of 20^0 and .02" offer the optimum design solution. Based on the parametric study, an optimal configuration for the proposed NOPV can be achieved. The final design specs are shown in Table 7.2. The tank has a .02"titainium liner with 75 filament layers of the nanocomposite fiber.

Table 7.2 NOPV Design Specifications

Tank Specifications	**Units**	**Spec**
Operating Pressure	MPa	31.026
Total Volume	cubic inches	4040
Design Wt.	lb	15.73
Dimensions	inches	15.76" DIA X 26.21" LONG
Ported Boss Wt[25].	lb	1.09
Stinger Boss Wt.[25]	lb	0.96
Film Adhesive Wt.[25]	lb	0.43
Titanium Liner Wall thickness	inches	0.02

CHAPTER 8

CONCLUSIONS AND FUTURE WORK

8.1 Conclusion

In conclusion, a NOPV has the potential to reduce structural mass of aerospace hardware because of its light weight and high stiffness properties. The results from the PAN-SWCNT/EPOXY micromechanics model were used to calculate the resulting mechanical properties of a lamina. A MATLAB code based on a simplified elasticity solution was developed and used to study the elastic behavior of an orthotropic COPV and NOPV when subjected to internal pressure. The results of the analyses showed that the PAN-SWCNT/EPOXY NOPV had stress-strain distributions that are similar to those of the T1000/EPOXY COPV.

The case study on the helium pressurization tank of the Messenger Spacecraft provided insight on the potential use of a NOPV. The results of the case study showed that under similar design parameters a NOPV could be used to reduce the spacecraft overall weight by 4.1 lb. Moreover, it was shown from the parametric study that the helical winding angle of the composite laminate and the thickness of the metallic liner play major roles in the stiffness and strength properties of a filament wound NOPV

structure. In addition, the results of the parametric study indicated that an optimum NOPV design specification could be achieved.

8.2 Future Work

As stated above, in order to simplify the analysis and also due to the lack of data, thermo-mechanical affects were neglected in the analysis. As more information is obtained about nanocomposite fibers, a future task is to perform analysis of NOPV under combined internal pressure and hygro-thermo loading. This analysis will yield important results that illustrate how a NOPV will handle induced environmental loads from temperature effects combined with moisture. Also, since the NOPV was analyzed as an alternating angle ply cylindrical laminate, it is important to explore other stacking sequences as well. The analysis would explore the effects of the different stacking sequences on the resulting stress/strain field of the titanium liner and composite overwrap.

APPENDICES

APPENDIX A

MATLAB PAN-SWCNT Micromechanics Model

```
function SWCNT_properties(Spreadsheet)

%guo_huina thesis pg. 49
vPAN=.07;
vCNT=.17;
%PAN/SWNT Volume fractions
Vf_f=.8;
Vf_m=.2;
%SWNT PAN Fiber properties from refferece is 17.8e9 GPa
%E1CNT_f=17.8e9;
ECNT=1e12;
E2CNT=15e9;
EPAN=7.9e9;
E1CNT_f=ECNT*Vf_f+EPAN*Vf_m;
GCNT=19.5e9;
GPAN=(EPAN)/(2*(1+vPAN))

Zq=2;
l_f=1;
d_f=20e-9;
%length over width for E1
QQ_1=4;
%Zq_1=2*(l_f/d_f)+40*(Vf_f)^(10);
Zq_1=2*(QQ_1)+40*(Vf_f)^(10);
% E2
Zq_2=2*(1)+40*(Vf_f)^(10);
% G12
Zq_3=1+40*(Vf_f)^(10);

E1CNT_f2=M_c2(ECNT,EPAN,.8,Zq_1);
E2CNT_f2=M_c2(E2CNT,EPAN,.8,Zq_2);
vCNT_f2=M_c2(vCNT,vPAN,.8,2);
GCNT_f2=M_c2(GCNT,GPAN,.8,Zq_3);

vCNT_f=vCNT*Vf_f+vPAN*Vf_m;
GCNT_f=E1CNT_f/(2*(1+vCNT_f));
```

```
%Code fix
E1CNT=E1CNT_f;


%SWNT PAN Fibers
E1f=E1CNT_f2
E2f=E2CNT_f2;
G33f=GCNT_f2;
v12f=vCNT_f2;

%Volume Fraction for laminate
Vf=.707;
Vm=1-Vf;

%Epoxy Matrix
Em=3.4e9;
E2m=Em;
G33m=1.308e9;
v12m=.34;

%My laminate
E1=E1f*Vf+Em*Vm;
%E1_q=M_c(E1f,Em,Vf);
%E2_q=M_c(E2f,E2m,Vf);
E2=(E1f*Em)/(E1f*Vm+Em*Vf);
E3=E2;
G33_q=M_c(G33f,G33m,Vf);
%G33=(G33f*G33m)/(G33f*Vm+G33m*Vf);
G33=1.3*(G33_q);
v12=v12f*Vf+v12m*Vm;
v21=v12;
%transveres young modulus
v23=v12f*Vf+v12m*(1-Vf)*(1+v12m-(v12*Em/E1))/(1-
(v12m^2)+v12m*v12*(Em/E1));

 Constants=[E1/1e9,E2/1e9,v12,v23,G33/1e9,Vf*100]';
xlswrite(Spreadsheet, Constants, 'Sheet1', 'E2:E7')
%Constants2=[E1/1e9,E2/1e9,v12,v23,G33/1e9,S1T_ult/1e6,S2T_ult/1e6,Tau12_ult/1e6
]';
%Constants2=[E1f/1e9,E2f/1e9,v12f]';

end
```

APPENDIX B

MATLAB Script

```
%Roosevelt Wright UAH
%Masters Dissertation Analysis Toolset


function HYY=M_c(Mf,Mm,Vf)

Zq=2;
Rratio=(Mf/Mm);
HY=(Rratio-1)/(Rratio+Zq);
HYY=Mm*(1+Zq*HY*Vf)/(1-HY*Vf);

function HYY=M_c2(Mf,Mm,Vf,Zq)

%Zq=2;
Rratio=(Mf/Mm);
HY=(Rratio-1)/(Rratio+Zq);
HYY=Mm*(1+Zq*HY*Vf)/(1-HY*Vf);

function SWCNT_properties2(Spreadsheet)

%guo_huina thesis pg. 49
vPAN=.07;
vCNT=.17;
%PAN/SWNT Volume fractions
Vf_f=.05;
Vf_m=1-Vf_f;
%SWNT PAN Fiber properties from refferece is 17.8e9 GPa
%E1CNT_f=17.8e9;

ECNT=1e12;
%ECNT=640e9;
E2CNT=15e9;
EPAN=7.9e9;
E1CNT_f=ECNT*Vf_f+EPAN*Vf_m;
GCNT=19.5e9;
GPAN=(EPAN)/(2*(1+vPAN))

Zq=2;
l_f=1;
d_f=20e-9;
```

```
%length over width for E1
QQ_1=4;
%Zq_1=2*(l_f/d_f)+40*(Vf_f)^(10);
Zq_1=2*(QQ_1)+40*(Vf_f)^(10);
% E2
Zq_2=2*(1)+40*(Vf_f)^(10);
% G12
Zq_3=1+40*(Vf_f)^(10);

E1CNT_f2=M_c2(ECNT,EPAN,Vf_f,Zq_1)/1e9
E2CNT_f2=M_c2(E2CNT,EPAN,.8,Zq_2);
vCNT_f2=M_c2(vCNT,vPAN,.8,2);
GCNT_f2=M_c2(GCNT,GPAN,.8,Zq_3);

vCNT_f=vCNT*Vf_f+vPAN*Vf_m;
GCNT_f=E1CNT_f/(2*(1+vCNT_f));

%Code fix
E1CNT=E1CNT_f/1e9


%SWNT PAN Fibers
E1f=E1CNT_f2
E2f=E2CNT_f2;
G33f=GCNT_f2;
v12f=vCNT_f2;


%Volume Fraction for laminate
Vf=.707;
Vm=1-Vf;


%Epoxy Matrix
Em=3.4e9;
E2m=Em;
G33m=1.308e9;
v12m=.34;


%My laminate
E1=E1f*Vf+Em*Vm;
%E1_q=M_c(E1f,Em,Vf);
%E2_q=M_c(E2f,E2m,Vf);
E2=(E1f*Em)/(E1f*Vm+Em*Vf);
E3=E2;
G33_q=M_c(G33f,G33m,Vf);
```

```
%G33=(G33f*G33m)/(G33f*Vm+G33m*Vf);
G33=1.3*(G33_q);
v12=v12f*Vf+v12m*Vm;
v21=v12;
%transveres young modulus
v23=v12f*Vf+v12m*(1-Vf)*(1+v12m-(v12*Em/E1))/(1-
(v12m^2)+v12m*v12*(Em/E1));


Constants=[E1/1e9,E2/1e9,v12,v23,G33/1e9,Vf*100]';
xlswrite(Spreadsheet, Constants, 'Sheet1', 'E2:E7')
%Constants2=[E1/1e9,E2/1e9,v12,v23,G33/1e9,S1T_ult/1e6,S2T_
ult/1e6,Tau12_ult/1e6]';
%Constants2=[E1f/1e9,E2f/1e9,v12f]';

end



function
[RSTR,CSTR,ASTR,GammaS_thz,RSR,CSR,ASR,Tthz,URadius,MRad...

,Tw_rateVV]=Thesis_Analysis(E1,E2,E3,G33,v12,v23,N,theta,P,
I_rad)


format short

% Input Parameters

Po=0;
F=0;
T=0;
dT=0;

%Length of Pressure Vessel [in]
L=10;
v21=v12;
v32=v23;


C_EP=[1/E1 -v21/E1 -v12/E1; -v21/E1 1/E2 -v32/E2; -v21/E1 -
v23/E2 1/E3;];
C_EP;
CEP=inv(C_EP);
```

```
%%Material Properties
Cxx=CEP(1,1);
Cxy=CEP(1,2);
Cxz=CEP(1,3);
Cyx=CEP(2,1);
Cyy=CEP(2,2);
Cyz=CEP(2,3);
Czx=CEP(3,1);
Czy=CEP(3,2);
Czz=CEP(3,3);
Gxx=E2/(2*(1+v23));
Gyy=G33;
Gzz=Gyy;



%Equation Parameter
M=N-1;

%%%%%%%%%%%%%%%%%%%%%%%%%%%%%%%%%%%%%%%%%%%%%%%%%%%%%%%%%%%%%%%%%%%%%%%
%%%%%%%%%%%%%%%
%%MATRIIX OPERATIONS Initializing the Angle Vector
%%%%%%%%%%%%%%%%%%%%%%%%%%%%%%%%%%%%%%%%%%%%%%%%%%%%%%%%%%%%%%%%%%%%%%%
%%%%%%%%%%%%%%%

%%MATRIIX OPERATIONS Initializing the Radius Vector
%%%%%%%%%%%%%%%%%%%%%%%%%%%%%%%%%%%%%%%%%%%%%%%%%%%%%%%%%%%%%%%%%%%%%%%
%%%%%%%%%%%%%%%
%Populating the radius vector
for n=0:N,
radset(n+1,1)=I_rad+n*(thickness);
end
ro=radset(N+1,1);
r=radset;
R11(1:N,1:100)=0;
for i=1:N,

    R11(i,:)=linspace(r(i,1),r(i+1,1),100);

end


%%%%%%%%%%%%%%%%%%%%%%%%%%%%%%%%%%%%%%%%%%%%%%%%%%%%%%%%%%%%%%%%%%%%%%%


%%%%%%%%%%%%%%%%%%%%%%%%%%%%%%%%%%%%%%%%%%%%%%%%%%%%%%%%%%%%%%%%%%%%%%%
%%%%%%%%%%%%%%%
```

```
%%MATRIIX OPERATIONS Stiffness Matrix
%%%%%%%%%%%%%%%%%%%%%%%%%%%%%%%%%%%%%%%%%%%%%%%%%%%%%%%%%%%%%%
%%%%%%%%%%%%%%%

E=[Cxx,Cyy,Czz,Cxy,Cxz,Cyz,Gxx,Gyy,Gzz]';


%%%%%%%%%%%%%%%%%%%%%%%%%%%%%%%%%%%%%%%%%%%%%%%%%%%%%%%%%%%%%%
%%%%%%%%%%%%%%%
%%MATRIIX OPERATIONS Using Transformation Matrix to obatin
the off-axis
%%stiffness
%%%%%%%%%%%%%%%%%%%%%%%%%%%%%%%%%%%%%%%%%%%%%%%%%%%%%%%%%%%%%%
%%%%%%%%%%%%%%%
C(1:13,N)=0;
 C_bar(1:13,N)=0;
for ii=1:N
    c=cosd(theta(ii,1));
    s=sind(theta(ii,1));

T_trsf=[ c.^4 s.^4 0 2.*(c.^2).*(s.^2) 0 0 0 0
4.*(c.^2).*(s.^2);...
(c.^2).*(s.^2) (c.^2).*(s.^2) 0 ((c.^4)+(s.^4)) 0 0 0 0 -
4.*(c.^2).*(s.^2);...
0 0 0 0 c.^2 s.^2 0 0 0;...
(c.^3).*s -c.*(s.^3) 0 ((-c.^3).*s+c.*(s.^3)) 0 0 0 0 ((-
2.*c.^3).*s+2.*c.*(s.^3));...
s.^4 c.^4 0 2.*(c.^2).*(s.^2) 0 0 0 0 4.*(c.^2).*(s.^2);...
0 0 0 0 s.^2 c.^2 0 0 0;...
(c.*s.^3) (-c.^3).*s 0 ((c.^3).*s-c.*(s.^3)) 0 0 0 0
((2.*c.^3).*s-2.*c.*(s.^3));...
0 0 1 0 0 0 0 0 0;...
0 0 0 0 c.*s -c.*s 0 0 0;...
0 0 0 0 0 0 c.^2 s.^2 0;...
0 0 0 0 0 0 -c.*s c.*s 0;...
0 0 0 0 0 0 s.^2 c.^2 0;...
(c.^2).*(s.^2) (c.^2).*(s.^2) 0 -2.*(c.^2).*(s.^2) 0 0 0 0
((c.^2)-(s.^2)).^2;];

%Obtaining New Stiffness Matrix
C=T_trsf*E;
%Taking all stiffness values and placing inside a matrix
wher each column
%represents a single laminae
C_bar(:,ii)=C;
end
```

```
%The off-axis stiffness constans calculated fromt the on-
axis stiffness
%constants
Gr_11=(100e9*(1-.3))/((1-2*.3)*(1+.3));
Gr_12=(100e9*.3)/((1-2*.3)*(1+.3));
C11(1:N,1)=Gr_11;
C12(1:N,1)=Gr_12;
C13(1:N,1)=Gr_12;
C16(1:N,1)=0;
C22(1:N,1)=Gr_11;
C23(1:N,1)=Gr_12;
C26(1:N,1)=0;
C33(1:N,1)=Gr_11;
C36(1:N,1)=0;
C44(1:N,1)=44e9;
C45(1:N,1)=0;
C55(1:N,1)=44e9;
C66(1:N,1)=44e9;


for ign=1:N-10
C11(11:N,1)=C_bar(1,ign)';
C12(11:N,1)=C_bar(2,ign)';
C13(11:N,1)=C_bar(3,ign)';
C16(11:N,1)=C_bar(4,ign)';
C22(11:N,1)=C_bar(5,ign)';
C23(11:N,1)=C_bar(6,ign)';
C26(11:N,1)=C_bar(7,ign)';
C33(11:N,1)=C_bar(8,ign)';
C36(11:N,1)=C_bar(9,ign)';
C44(11:N,1)=C_bar(10,ign)';
C45(11:N,1)=C_bar(11,ign)';
C55(11:N,1)=C_bar(12,ign)';
C66(11:N,1)=C_bar(13,ign)';

end

%%%%%%%%%%%%%%%%%%%%%%%%%%%%%%%%%%%%%%%%%%%%%%%%%%%%%%%%%%%%%%%%%%%%%%%%
%%%%%%%%%%%%%%%%
%%MATRIIX OPERATIONS Finding Lamda for the various Laminae
%%%%%%%%%%%%%%%%%%%%%%%%%%%%%%%%%%%%%%%%%%%%%%%%%%%%%%%%%%%%%%%%%%%%%%%%
%%%%%%%%%%%%%%%%
q=1:N;
beta(q,1)=0;
for qq=1:N,
beta=sqrt(C22(1:N,1)./C33(1:N,1));
end
```

```
beta(1:10,1)=1;
%%%%%%%%%%%%%%%%%%%%%%%%%%%%%%%%%%%%%%%%%%%%%%%%%%%%%%%%%%%
%%%%%%%%%%%%%%%



%%%%%%%%%%%%%%%%%%%%%%%%%%%%%%%%%%%%%%%%%%%%%%%%%%%%%%%%%%%
%%%%%%%%%%%%%%%
%%MATRIIX OPERATIONS Finding alpha1,alpha2
%%%%%%%%%%%%%%%%%%%%%%%%%%%%%%%%%%%%%%%%%%%%%%%%%%%%%%%%%%%
%%%%%%%%%%%%%%%

alpha1=(C12(1:N,1)-C13(1:N,1))./(C33(1:N,1)-C22(1:N,1));
alpha2=(C26(1:N,1)-2.*C36(1:N,1))./(4.*C33(1:N,1)-
C22(1:N,1));

alpha1(1:10,1)=0;
alpha2(1:10,1)=0;
%%%%%%%%%%%%%%%%%%%%%%%%%%%%%%%%%%%%%%%%%%%%%%%%%%%%%%%%%%%
%%%%%%%%%%%%%%%
alpha1(isnan(alpha1)) = 0;
alpha2(isnan(alpha2)) = 0;
%%%%%%%%%%%%%%%%%%%%%%%%%%%%%%%%%%%%%%%%%%%%%%%%%%%%%%%%%%%
%%%%%%%%%%%%%%%
%%MATRIIX OPERATIONS Finding K1,K2,K3,K4
%%%%%%%%%%%%%%%%%%%%%%%%%%%%%%%%%%%%%%%%%%%%%%%%%%%%%%%%%%%
%%%%%%%%%%%%%%%



%%%%%%%%%%%%%%%%%%%%%%%%%%%%%%%%%%%%%%%%%%%%%%%%%%%%%%%%%%%
%%%%%%%%%%%%%%%
%%MATRIIX OPERATIONS Setting the A Matrix
%%%%%%%%%%%%%%%%%%%%%%%%%%%%%%%%%%%%%%%%%%%%%%%%%%%%%%%%%%%
%%%%%%%%%%%%%%%
%Setting First Row
i=1:2*N+2;
%Intialize Matrix
A(i,i)=0;
%Setting First Term
A(1,1)=(C23(1,1)+beta(1,1).*C33(1,1)).*I_rad.^(beta(1,1)-
1);

%Setting constants in Matrix for the Internal Pressure
Equation
A(1,1+N)=(C23(1,1)-beta(1,1).*C33(1,1)).*I_rad.^(-
beta(1,1)-1);
```

```
 %C1
A(1,2+N+M)=C13(1,1)+alpha1(1,1).*(C23(1,1)+C33(1,1));
A(1,3+N+M)=(C36(1,1)+alpha2(1,1).*(C23(1,1)+2.*C33(1,1))).*
I_rad;

%Setting new Radius "Had to add this for my code to work
%r(1,1)=.0505;
%r(2,1)=.051;
%r(3,1)=.0515;
%r(4,1)=.052;

for jac=1:N,

    r(jac,1)=r(jac+1,1);

end

%%%%%%%%%%%%%%%%%%%%%%%%%%%%%%%%%%%%%%%%%%%%%%%%%%%%%%%%%%%%%%%%%%%%%%%
%%%%%%%%%%%%%%%
%Getting the Displacement Coeficcents from displacement
Equation
%%%%%%%%%%%%%%%%%%%%%%%%%%%%%%%%%%%%%%%%%%%%%%%%%%%%%%%%%%%%%%%%%%%%%%%
%%%%%%%%%%%%%%%

% Getting the A integration Constants
for j=0:M-1,

    A(j+2,j+1)=r(j+1,1).^beta(j+1,1);

end

for e=1:M,

    %A(e+1,e+1)=-(r(e+1,1).^beta(e+1,1));
        A(e+1,e+1)=-(r(e,1).^beta(e+1,1));

end

for je=0:M-1,
%Getting C1 and E the strains
A(je+2,2+N+M)=(alpha1(je+1,1)-alpha1(je+1+1,1)).*r(je+1,1);
A(je+2,3+N+M)=(alpha2(je+1,1)-
alpha2(je+1+1,1)).*r(je+1,1).^2;
end

%Getting the B integration Constants
for jj=0:M-1,
```

```
    %A(jj+2,jj+N+1)=(r(jj+1,1).^beta(jj+1,1));
    A(jj+2,jj+N+1)=(r(jj+1,1).^-beta(jj+1,1));

end

for ee=1:M,

   % A(ee+1,ee+N+1)=-(r(ee,1).^-beta(ee+1,1));
      A(ee+1,ee+N+1)=-(r(ee,1).^-beta(ee+1,1));

end
%%%%%%%%%%%%%%%%%%%%%%%%%%%%%%%%%%%%%%%%%%%%%%%%%%%%%%%%%%%%%%

%%%%%%%%%%%%%%%%%%%%%%%%%%%%%%%%%%%%%%%%%%%%%%%%%%%%%%%%%%%%%%
%%%%%%%%%%%%%%%
%Using Radial Stress Equation
%%%%%%%%%%%%%%%%%%%%%%%%%%%%%%%%%%%%%%%%%%%%%%%%%%%%%%%%%%%%%%
%%%%%%%%%%%%%%%

% Getting the A integration Constants

for j=0:M-1,
A(N+j+1,j+1)=(C23(j+1,1)+beta(j+1,1).*C33(j+1,1)).*r(j+1,1)
.^(beta(j+1,1)-1);

end

for e=1:M,

A(M+e+1,e+1)=-
(C23(e+1,1)+beta(e+1,1).*C33(e+1,1)).*r(e,1).^(beta(e+1,1)-
1);

end

%Getting C1 and E the strains
%added another 1
for jer=0:M-1,

A(N+jer+1,2+N+M)=(C13(jer+1,1)-
C13(jer+1+1,1))+alpha1(jer+1,1).*...
    (C23(jer+1,1)+C33(jer+1,1))-
alpha1(jer+1+1).*(C23(jer+1+1,1)...
    +C33(jer+1+1,1));
A(N+jer+1,3+N+M)=((C36(jer+1,1)-
C36(jer+1+1,1))+alpha2(jer+1,1).*...
```

```
    (C23(jer+1,1)+2.*C33(jer+1,1))-
alpha2(jer+1+1).*(C23(jer+1+1,1)...
    +2.*C33(jer+1+1,1))).*r(jer+1,1);

end

%Getting the B integration Constants
for jj=0:M-1,

    A(jj+N+1,jj+N+1)=(C23(jj+1,1)-beta(jj+1,1).*...
        C33(jj+1,1)).*r(jj+1,1).^(-beta(jj+1,1)-1);

end

for ee=1:M,

    A(M+ee+1,ee+N+1)=-(C23(ee+1,1)-
beta(ee+1,1).*C33(ee+1,1)).*...
        r(ee,1).^(-beta(ee+1,1)-1);

end
%%%%%%%%%%%%%%%%%%%%%%%%%%%%%%%%%%%%%%%%%%%%%%%%%%%%%%%%%%%%%%%%%%%%%%%

%%%%%%%%%%%%%%%%%%%%%%%%%%%%%%%%%%%%%%%%%%%%%%%%%%%%%%%%%%%%%%%%%%%%%%%
%%%%%%%%%%%%%%%%
%Setting Radial Stress to External Pressure Equation
%%%%%%%%%%%%%%%%%%%%%%%%%%%%%%%%%%%%%%%%%%%%%%%%%%%%%%%%%%%%%%%%%%%%%%%
%%%%%%%%%%%%%%%%

% Getting the A integration Constants
A(2*N,N)=(C23(N,1)+beta(N,1).*C33(N,1)).*ro.^(beta(N,1)-1);

%Getting the B integration Constants
A(2*N,1+N+M)=(C23(N,1)-beta(N,1).*C33(N,1)).*ro.^(-
beta(N,1)-1);

%Getting C1 and E the strains
A(2*N,2+N+M)=C13(N,1)+alpha1(N,1).*(C23(N,1)+C33(N,1));

A(2*N,3+N+M)=(C36(N,1)+alpha2(N,1).*(C23(N,1)+2.*C33(N,1)))
.*ro;

%%%%%%%%%%%%%%%%%%%%%%%%%%%%%%%%%%%%%%%%%%%%%%%%%%%%%%%%%%%%%%%%%%%%%%%


%%%%%%%%%%%%%%%%%%%%%%%%%%%%%%%%%%%%%%%%%%%%%%%%%%%%%%%%%%%%%%%%%%%%%%%
%%%%%%%%%%%%%%%%
```

```
%Using Axial Loading Equation
%%%%%%%%%%%%%%%%%%%%%%%%%%%%%%%%%%%%%%%%%%%%%%%%%%%%%%%%%%%%
%%%%%%%%%%%%%%%

 %r=[.05 .0505 .051 .0515 .052]';
 r=radset;
% Getting the A integration Constants

for jy=1:N,


A(2*N+1,jy)=((C12(jy)+(beta(jy).*C13(jy)))./(1+beta(jy))).*
(r(jy+1).^...
        (beta(jy)+1)-r(jy).^(beta(jy)+1));

end

%Getting the B integration Coefficents
for uy=1:N,
A(2*N+1,N+uy)=((C12(uy)-(beta(uy).*C13(uy)))./(1-
beta(uy))).*(r(uy+1).^...
    (-beta(uy)+1)-r(uy).^(-beta(uy)+1));
end

%Getting C1 and E the strains
%Intializing AC1 Vector
ui=1:N;
AC1(ui,1)=0;

for ky=1:N,

AC1(ky,1)=(C11(ky,1)+alpha1(ky,1).*(C12(ky,1)+C13(ky,1))).*
...
        ((r(ky+1,1).^2-r(ky,1).^2)./2);

end
%Intializing Aez Vector
ud=1:N;
AEz(ud,1)=0;

for rp=1:N,

AEz(rp,1)=(C16(rp,1)+alpha2(rp,1).*(C12(rp,1)+2.*C13(rp,1))
).*...
        (r(rp+1,1).^3-r(rp,1).^3)./3;

end
```

```
A(2*N+1,2+N+M)=sum(AC1);
A(2*N+1,3+N+M)=sum(AEz);

%%%%%%%%%%%%%%%%%%%%%%%%%%%%%%%%%%%%%%%%%%%%%%%%%%%%%%%%%%%%%

%%%%%%%%%%%%%%%%%%%%%%%%%%%%%%%%%%%%%%%%%%%%%%%%%%%%%%%%%%%%%
%%%%%%%%%%%%%%%
%Using Moment/Torque Loading Equation
%%%%%%%%%%%%%%%%%%%%%%%%%%%%%%%%%%%%%%%%%%%%%%%%%%%%%%%%%%%%%
%%%%%%%%%%%%%%%

% Getting the A integration Constants
%for ey=N+1:2*N,
for rd=1:N,
A(2*N+2,rd)=((C26(rd)+(beta(rd).*C36(rd)))/(2+beta(rd))).*(
r(rd+1).^...
    (beta(rd)+2)-r(rd).^(beta(rd)+2));

end

%Getting the B integration Constants
for ed=N+1:2*N,
A(2*N+2,ed)=((C26(ed-N)-(beta(ed-N).*C36(ed-N)))/(2-
beta(ed-N))).*...
    (r(ed-N+1).^(-beta(ed-N)+2)-r(ed-N).^(-beta(ed-N)+2));

end

%Getting C1 and E the strains


%Intializing TAC1 Vector
tui=1:N;
TAC1(tui,1)=0;
for tp=1:N,

TAC1(tp,1)=(C16(tp,1)+alpha1(tp,1).*(C26(tp,1)+C36(tp,1))).
*...
        (r(tp+1,1).^3-r(tp,1).^3)./3;

end

TAC1;

%Intializing TAez Vector
tud=1:N;
```

```
TAEz(tud,1)=0;
for kt=1:N,


TAEz(kt,1)=(C66(kt,1)+alpha2(kt,1).*(C26(kt,1)+2.*C36(kt,1)
)).*...
        (r(kt+1,1).^4-r(kt,1).^4)./4;

 end

A(2*N+2,2+N+M)=sum(TAC1);
A(2*N+2,3+N+M)=sum(TAEz);
%%%%%%%%%%%%%%%%%%%%%%%%%%%%%%%%%%%%%%%%%%%%%%%%%%%%%%%%%%%%%%%%%%%%%%%%
%%%%%%%%%%%%%%

%%%%%%%%%%%%%%%%%%%%%%%%%%%%%%%%%%%%%%%%%%%%%%%%%%%%%%%%%%%%%%%%%%%%%%%%
%%%%%%%%%%%%%%
%%MATRIIX OPERATIONS Setting the solution Matrix
%%%%%%%%%%%%%%%%%%%%%%%%%%%%%%%%%%%%%%%%%%%%%%%%%%%%%%%%%%%%%%%%%%%%%%%%
%%%%%%%%%%%%%%
%Initialize Vector
B(i,1)=0;
%Internal Pressure
B(1,1)=-P;
%External Pressure
B(2*N,1)=0;
%Axial Loading Equation
B(2*N+1,1)=P*I_rad^2/(2);
%Moment/Torque Loading
B(2*N+2,1)=0;

%Normalizing Matrix

%Solution Vector

ir= find(isnan(A)); %
A(ir)= zeros(size(ir));

% 1.  Determine the absolute maximum value for each row in
the matrix A:
saa=max(abs(A'))';

% 2.  Set any 0 that you obtain for a rows absolute maximum
...
%value by 1 since you will be dividing by this value.
saa(find(saa==0))=1;
% 3.  Divide the matix A by its absolute maximum value:
```

```
A=diag(saa)\A;

B=B./saa;

%A(isnan(A)) = 0;
I_bar=A\B;
A_Int=I_bar(1:N,1);
B_Int=I_bar(N+1:2*N,1);
%C1_Int=I_bar(2*N+1,1);
%e_Int=I_bar(2*N+2,1);
C1_Int=I_bar(2*N+2,1);
e_Int=I_bar(2*N+1,1);

%%%%%%%%%%%%%%%%%%%%%%%%%%%%%%%%%%%%%%%%%%%%%%%%%%%%%%%%%%%%%%%%%%%%%%%
%%%%%%%%%%%%%%%%%%%%%%%%%%%%%%%%%%%%%%%%%%%%%%%%%%%%%%%%%%%%%%%%%%%%%%%
%%MATRIIX OPERATIONS Finding the displacement and strains
in each laminate
%%%%%%%%%%%%%%%%%%%%%%%%%%%%%%%%%%%%%%%%%%%%%%%%%%%%%%%%%%%%%%%%%%%%%%%
%%%%%%%%%%%%%%%%%%%%%%%%%%%%%%%%%%%%%%%%%%%%%%%%%%%%%%%%%%%%%%%%%%%%%%%
int=1:N;
U_r(1:N,1:100)=0;
U_c(1:N,1:100)=0;
U_ax(1:N,1:100)=0;
E_r(1:N,1:100)=0;
E_th(1:N,1:100)=0;
E_z(1:N,1:100)=0;
Gamma_thz(1:N,1:100)=0;
Gamma_rz(1:N,1:100)=0;
Gamma_rth(1:N,1:100)=0;
Z(int,1)=L;

 for fk=1:N,

    r=radset;
    %Displacements in radial Direction

U_r(fk,1:100)=A_Int(fk,1).*R11(fk,1:100).^beta(fk,1)+B_Int(
fk,1).*...
        R11(fk,1:100).^(-
beta(fk,1))+alpha1(fk,1).*e_Int.*R11(fk,1:100)...
        +alpha2(fk,1).*C1_Int(1,1).*R11(fk,1:100).^2;
      %Displacements in Circumferential Direction
    U_c(fk,1:100)=R11(fk,1:100).*Z(fk,1).*C1_Int(1,1);
    %Displacements in axial Direction
    U_ax(fk,1:100)=Z(fk,1).*e_Int;
```

```
    %Strain in radial Direction


   E_r(fk,1:100)=-(-
A_Int(fk,1).*(R11(fk,1:100).^beta(fk,1)).*...
       beta(fk,1)+B_Int(fk,1).*(R11(fk,1:100).^(-
beta(fk,1))).*...
       beta(fk,1)-alpha1(fk,1).*e_Int.*R11(fk,1:100)-
2.*alpha2(fk,1).*...
       (R11(fk,1:100).^2).*C1_Int(1,1))./R11(fk,1:100);
    %Strain in cicumferential Direction
    E_th(fk,1:100)=U_r(fk,1:100)./R11(fk,1:100);
    %Strain in the Axial Direction
    E_z(fk,1:100)=e_Int(1,1);
    %Shear Strain in the theta z direction
    Gamma_thz(fk,1:100)=R11(fk,1:100).*C1_Int(1,1);
   %Twist Rate

end

%%%%%%%%%%%%%%%%%%%%%%%%%%%%%%%%%%%%%%%%%%%%%%%%%%%%%%%%%%%%%%%%%%%%%%%%
%%%%%%%%%%%%%%
%%MATRIIX OPERATIONS Finding the stresses in each laminate
%%%%%%%%%%%%%%%%%%%%%%%%%%%%%%%%%%%%%%%%%%%%%%%%%%%%%%%%%%%%%%%%%%%%%%%%
%%%%%%%%%%%%%%


S_r(1:N,1:100)=0;
S_th(1:N,1:100)=0;
S_z(1:N,1:100)=0;
Tau_thz(1:N,1:100)=0;
Tau_rz(1:N,1:100)=0;
Tau_rth(1:N,1:100)=0;

for yk=1:N,
     %  r=[0 0 0 0 0]';
  %Radial Stress

S_r(yk,1:100)=C13(yk,1).*E_z(yk,1:100)+C23(yk,1).*E_th(yk,1
:100)+...

C33(yk,1).*E_r(yk,1:100)+C36(yk,1).*Gamma_thz(fk,1:100);
     %Circuferentail strss

S_th(yk,1:100)=C12(yk,1).*E_z(yk,1:100)+C22(yk,1).*E_th(yk,
1:100)+...
```

```
C23(yk,1).*E_r(yk,1:100)+C26(yk,1).*Gamma_thz(fk,1:100);
      %Axial Stress

S_z(yk,1:100)=C11(yk,1).*E_z(yk,1:100)+C12(yk,1).*E_th(yk,1
:100)+...

C13(yk,1).*E_r(yk,1:100)+C16(yk,1).*Gamma_thz(fk,1:100);
      %Shear Stress in the Circuferential a axial plane

Tau_thz(yk,1:100)=C16(yk,1).*E_z(yk,1:100)+C26(yk,1).*E_th(
yk,1:100)+...

C36(yk,1).*E_r(yk,1:100)+C66(yk,1).*Gamma_thz(fk,1:100);
     %Shear Stress in the radial and axial plane
    Tau_rz(yk,1:100)=0;
 %Shear Stress in the Circuferential and radial plane
    Tau_rth(yk,1:100)=0;

end
  SS_r(1,1:100)=0;

SS_r(1,1:100)=C13(3,1).*E_z(3,1:100)+C23(3,1).*E_th(3,1:100
)+...

C33(3,1).*E_r(3,1:100)+C36(3,1).*Gamma_thz(3,1:100);




%%%%%%%%%%%%%%%%%%%%%%%%%%%%%%%%%%%%%%%%%%%%%%%%%%%%%%%%%%%%%%%%%%%%%%%
%%%%%%%%%%%%%%

%%%%%%%%%%%%%%%%%%%%%%%%%%%%%%%%%%%%%%%%%%%%%%%%%%%%%%%%%%%%%%%%%%%%%%%
%%%%%%%%%%%%%%

R(1:N,1)=0;
for rdim=1:N;
    R(rdim,1)=(r(rdim)-I_rad)./(r(4,1)-I_rad);
end


 %Collecting Results
  Radial_Strain_results=reshape(E_r',1,100*N);
  Circum_Strain_results=reshape(E_th',1,100*N);
  Axial_Strain_results=reshape(E_z',1,100*N);
  Shear_Strain_results=reshape(Gamma_thz',1,100*N);
```

```
  Radial_Strss_results=reshape(S_r',1,100*N);
  Circum_Strss_results=reshape(S_th',1,100*N);
  Axial_Strss_results=reshape(S_z',1,100*N);
  Shear_Stress_results=reshape(Tau_thz',1,100*N);
  radial_deflection_results=reshape(U_r',1,100*N);
  Radius_Combined=reshape(R11',1,100*N);


  RSTR=Radial_Strain_results';
  CSTR=Circum_Strain_results';
  ASTR=Axial_Strain_results';
  GammaS_thz=Shear_Strain_results';
  RSR=Radial_Strss_results';
  CSR=Circum_Strss_results';
  ASR=Axial_Strss_results';
  Tthz=Shear_Stress_results';
  URadius=radial_deflection_results';
  MRadius=Radius_Combined';
  %MRadius=linspace(I_rad,ro,length(RSR));

  MRad(1:length(MRadius),1)=0;
for rdim=1:length(RSR);
    MRad(rdim,1)=(MRadius(rdim)-I_rad)./(ro-I_rad);
end

Constants_CaseA=[RSTR.*1e6,ASTR.*1e6,CSTR.*1e6,RSR./1e6,ASR
./1e6,...
    CSR./1e6,MRad,Tthz./1e6,1000*URadius];

 %Twist Rate converted to Degrees Per mm
Tw_rate=1e6*(C1_Int*(57.23/1000));
Tw_rateV(1:100*N,1)=Tw_rate;
Tw_rateVV=Tw_rateV';
%SWCNT


function createfigurewithsubs(X1, Y1, Y2, Y3)
%CREATEFIGURE(X1,Y1,Y2,Y3)
%  X1:  vector of x data
%  Y1:  vector of y data
%  Y2:  vector of y data
%  Y3:  vector of y data

%  Auto-generated by MATLAB on 19-Jul-2009 16:13:35

% Create figure
figure1 = figure('Color',[1 1 1]);
```

```
% Create subplot
subplot1 = subplot(3,1,1,'Parent',figure1);
box('on');
hold('all');

% Create plot
plot(X1,Y1,'Parent',subplot1);

% Create xlabel
xlabel('R');

% Create ylabel
ylabel('generic axis');

% Create zlabel
zlabel({'',''},'Visible','off');

% Create subplot
subplot2 = subplot(3,1,2,'Parent',figure1);
box('on');
hold('all');

% Create plot
plot(X1,Y2,'Parent',subplot2);

% Create xlabel
xlabel('R');

% Create ylabel
ylabel('generic axis');

% Create subplot
subplot3 = subplot(3,1,3,'Parent',figure1);
box('on');
hold('all');

% Create plot
plot(X1,Y3,'Parent',subplot3);

% Create xlabel
xlabel('R');

% Create ylabel
ylabel('generic axis');

% Create legend
```

```
legend(subplot1,'show');

% Create legend
legend(subplot2,'show');

% Create legend
legend(subplot3,'show');

% Create textbox
annotation(figure1,'textbox',[0.1321 0.8766 0.09371
0.05082],...
    'String',{'TYPE-A'},...
    'HorizontalAlignment','center',...
    'FontWeight','bold',...
    'FitBoxToText','off');

% Create textbox
annotation(figure1,'textbox',[0.1322 0.5735 0.09599
0.05082],...
    'String',{'TYPE-B'},...
    'HorizontalAlignment','center',...
    'FontWeight','bold',...
    'FitBoxToText','off');

% Create textbox
annotation(figure1,'textbox',[0.1319 0.2722 0.09371
0.05082],...
    'String',{'TYPE-C'},...
    'FontWeight','bold');
```

APPENDIX C

MATLAB Winding Angle Optimization Script

```
Number_L=10+85;
N=Number_L;
P=31.26e6;
Po=0;
F=0;
T=0;
dT=0;
%angle=45;
%Internal Radius [m]
I_rad=.2;
%Thickness of ply [m]
thickness=5.08e-5;
L=10;
%t=55;

angle=[10,15,20,25,30,35,40,45,50,55,60,65,70,75,80]';

%cndt_1=1;
for i=1:15
[y1AA,y3AA,y4AA]=CylindricalPV_PAngle(Number_L,P,F,T,I_rad,thickness,L,angle(i
,1));

%Baseline Liner
[T8HVAL(i,:),TPHVAL(i,:)]=Liner_PAngle(N,y1AA,y3AA,y4AA);
%Baseline composite
[T8HVC(i,:),TPHVAC(i,:)]=PANT1000_PAngle(N,y1AA,y3AA,y4AA);

end



%report ('My Plots2.rpt')


function [y1,y3,y4]=CylindricalPV_PAngle(Number_L,P,F,T,I_rad,thickness,L,theta)
```

```
%num = xlsread(filename, sheet, 'range')
E1=xlsread('data.xls', 'lookup', 'B2:B5').*1e9;
E2=xlsread('data.xls', 'lookup', 'C2:C5').*1e9;
E3=xlsread('data.xls', 'lookup', 'C2:C5').*1e9;
G33=xlsread('data.xls', 'lookup', 'F2:F5').*1e9;
v12=xlsread('data.xls', 'lookup', 'D2:D5');
v23=xlsread('data.xls', 'lookup', 'E2:E5');


for i=1:2;


[RSTR(i,:),CSTR(i,:),ASTR(i,:),GammaS_thz(i,:),RSR(i,:),CSR(i,:),ASR(i,:),Tthz(i,:),U
Radius(i,:),MRad(i,:),Tw_rate(i,:)]=Thesis_Analysis_PAngle(E1(i,1),E2(i,1),E3(i,1),G33
(i,1),v12(i,1),v23(i,1),Number_L,P,I_rad,theta);

end

for ii=1:2;
y1(ii,:)=RSR(ii,:)./1e6;
y2(ii,:)=ASR(ii,:)./1e6;
y3(ii,:)=CSR(ii,:)./1e6;
y4(ii,:)=GammaS_thz(ii,:)./1e6;
y5(ii,:)=RSTR(ii,:).*1e6;
y6(ii,:)=ASTR(ii,:).*1e6;
y7(ii,:)=CSTR(ii,:).*1e6;
y8(ii,:)=Tthz(ii,:).*1e6;
y9(ii,:)=URadius(ii,:).*1000;
y10(ii,:)=Tw_rate(ii,:);
y11(ii,:)=(CSR(ii,:)./1e6)./(ASR(ii,:)./1e6);
end




LME1={'radial stress ' 'axial stress ' 'circumferential stress ' 'shear stress'}';
LME2={'radial strain ' 'axial strain ' 'circumferential strain ' 'shear strain'}';




function [Ak,Bk]=Liner_PAngle(N,y1AA,y3AA,y4AA)
```

```
%Analyizing T800 and PAN for tsai hill
   for i=0:N-86;
%Radial Streess Y1
rad1A=max(abs(y1AA(1:2,(i*100)+1:(i+1)*100)'));


%Circoumferential Stress Y3
CCMA=max(abs(y3AA(1:2,(i*100)+1:(i+1)*100)'));


%Shear Stress S12 Y4
SShA=max(abs(y4AA(1:2,(i*100)+1:(i+1)*100)'));


%[mp]=tsai_hill(S1,S2,S12);

ThA81(i+1)=rad1A(1,1).*1e6;
ThA83(i+1)=CCMA(1,1).*1e6;
ThA84(i+1)=SShA(1,1).*1e6;



PANAth1(i+1)=rad1A(1,2).*1e6;
PANAth3(i+1)=CCMA(1,2).*1e6;
PANAth4(i+1)=SShA(1,2).*1e6;


%For the T800
[mpA800(i+1),T8HVA(i+1)]=tsai_hill2(ThA81(i+1),ThA83(i+1),ThA84(i+1));


%For the PAN
[mpAPAN(i+1),TPHVA(i+1)]=tsai_hill2(PANAth1(i+1),PANAth3(i+1),PANAth4(i+1))
;


end

Ak=max(T8HVA')
Bk=max(TPHVA')
%Toray


function [Ak,Bk]=PANT1000_PAngle(N,y1AA,y3AA,y4AA)
%Analyizing T800 and PAN for tsai hill
for i=0:N-11;
```

```
%Radial Streess Y1
rad1A=max(abs(y1AA(1:2,1001+(i*100):1000+(i+1)*100)'));

%Circoumferential Stress Y3
CCMA=max(abs(y3AA(1:2,1001+(i*100):1000+(i+1)*100)'));


%Shear Stress S12 Y4
SShA=max(abs(y4AA(1:2,1001+(i*100):1000+(i+1)*100)'));

%[mp]=tsai_hill(S1,S2,S12);

ThA81(i+1)=rad1A(1,1).*1e6;
ThA83(i+1)=CCMA(1,1).*1e6;
ThA84(i+1)=SShA(1,1).*1e6;


PANAth1(i+1)=rad1A(1,2).*1e6;
PANAth3(i+1)=CCMA(1,2).*1e6;
PANAth4(i+1)=SShA(1,2).*1e6;



%For the T800
[mpA800(i+1),T8HVA(i+1)]=tsai_hill(ThA81(i+1),ThA83(i+1),ThA84(i+1));

%For the PAN
[mpAPAN(i+1),TPHVA(i+1)]=tsai_hill(PANAth1(i+1),PANAth3(i+1),PANAth4(i+1));

end

Ak=max(T8HVA')
Bk=max(TPHVA')
```

APPENDIX D

MATLAB Liner Thickness Optimization Script

```
function
[TPHVAL,TPHVAC]=CylindricalPV_Pliner(N,P,F,T,I_rad,thickness,L,theta,liner_count
)


%num = xlsread(filename, sheet, 'range')
E1=xlsread('data.xls', 'lookup', 'B2:B5').*1e9;
E2=xlsread('data.xls', 'lookup', 'C2:C5').*1e9;
E3=xlsread('data.xls', 'lookup', 'C2:C5').*1e9;
G33=xlsread('data.xls', 'lookup', 'F2:F5').*1e9;
v12=xlsread('data.xls', 'lookup', 'D2:D5');
v23=xlsread('data.xls', 'lookup', 'E2:E5');


for i=1:2;


[RSTR(i,:),CSTR(i,:),ASTR(i,:),GammaS_thz(i,:),RSR(i,:),CSR(i,:),ASR(i,:),Tthz(i,:),U
Radius(i,:),MRad(i,:),Tw_rate(i,:)]=Thesis_Analysis_Pliner(E1(i,1),E2(i,1),E3(i,1),G33(i
,1),v12(i,1),v23(i,1),N,P,I_rad,theta,liner_count);

end

for ii=1:2;
y1(ii,:)=RSR(ii,:)./1e6;
y2(ii,:)=ASR(ii,:)./1e6;
y3(ii,:)=CSR(ii,:)./1e6;
y4(ii,:)=GammaS_thz(ii,:)./1e6;
y5(ii,:)=RSTR(ii,:).*1e6;
y6(ii,:)=ASTR(ii,:).*1e6;
y7(ii,:)=CSTR(ii,:).*1e6;
y8(ii,:)=Tthz(ii,:).*1e6;
y9(ii,:)=URadius(ii,:).*1000;
y10(ii,:)=Tw_rate(ii,:);
y11(ii,:)=(CSR(ii,:)./1e6)./(ASR(ii,:)./1e6);
end
```

```
TPHVAL=Liner_Pliner(N,y1,y3,y4,liner_count);
TPHVAC=PANT1000_Pliner(N,y1,y3,y4,liner_count);

P=31.26e6;
Po=0;
F=0;
T=0;
dT=0;

%Internal Radius [m]
I_rad=.2;
%Thickness of ply [m]
thickness=5.08e-5;
L=10;
liner_count=[11,12,13,14,15]';
disp('Orders recieved and understood')
  disp('engaging.....   ')
for k=1:5
N=60:240;
   for i=1:length(N)

[TPHVAL(i,:),TPHVAC(i,:)]=CylindricalPV_Pliner(N(i),P,F,T,I_rad,thickness,L,20,line
r_count(k,1));

   end
   Liner(:,k)=[TPHVAL];
   Composite(:,k)=[TPHVAC];
   %disp(['Completed Liner Equivalent thickness of ' int2str(liner_count(k,1)) ' lamina.'])
   disp(['Completed Liner Equivalent thickness of ' int2str(k+4) ' lamina.'])
end
 disp('All Clear Commander')

  disp('Proceeding to seceondary objective.....')
 A=0;
 B=0;

 for ij=1:5
  ii=0;
  disp(['Liner thickness: ' num2str(liner_count(ij,1))])
while A<=0 & B<=1.2
   A=1-Composite(ii+1,ij);
   B=(880./Liner(ii+1,ij))-1.2;
    ii=ii+1;
        %disp(['x= ' num2str(x)])
```

```
  disp(['Total Number of layers needed:' num2str(N(ii))])
 end

%end


 end

  disp('   ')
     disp('   ')
 disp('In position standing by.....')
```

REFERENCES

[1] Humble, R.W. *Propulsion analysis and design.* McGraw-Hill, 1995, p. 214.

[2] http://www.aussieinvader.com/Rocket_engines.php

[3] http://www.psi-pci.com/Data_Sheets_Library/DS386-101.pdf

[4] http://www.psi-pci.com/Data_Sheets_Library/DS436.pdf

[5] http://www.psi-pci.com/Technical_Paper_Library/AIAA%202003-4606%20Star2%20fuel.pdf

[6] Liang, J. *Single wall carbon nanotube/polyacrylonitrile composite fiber*, M.S. Thesis, Georgia Institute of Technology, 2004.

[7] http://www.pa.msu.edu/cmp/csc/ntproperties/equilibriumstructure.html

[8] http://ipn2.epfl.ch/CHBU/NTbasics1.htm

[9] http://en.wikipedia.org/wiki/Carbon_nanotube

[10] http://www.cems.umn.edu/~hsuhan/presentation_files/shortened_version.ppt

[11] Kaw, K. *Mechanics of composite materials*. CRC Press, 2006, p. 18, 208.

[12] Jones, R. M. *Mechanics of composite materials*. McGraw-Hill, 1975, p. 214.

[13] Guo, G. *Structure, processing, and properties of polyacrylonitrile/carbon nanotubes composite films*, Ph.D. Thesis, Georgia Institute of Technology, 2007, p. 49.

[14] Peters, S.T. *Handbook of composites.* Springer, 1998, p. 761.

[15] Tutuncu, N, and S J. Winckler. "Stresses and Deformations in Thick-Walled Cylinders Subjected to Combined Loading and a Temperature Gradient." *Journal of Reinforced Plastics and Composites* 12, no. 2 (1993): 198-209.

[16] Xia, M., H. Takayanagi, and K. Kemmochi. "Analysis of multi-layered filament-wound composite pipes under internal pressure." *Composite Structures* 53, no. 4 (2001): 483-491.

[17] Kobayashi, S., T. Imai, and S. Wakayama. "Burst strength evaluation of the FW-CFRP hybrid composite pipes considering plastic deformation of the liner." *Composites Part A: Applied Science and Manufacturing* 38, no. 5 (2007): 1344-1353.

[18] http://www.messenger-education.org/mission/mission_index.php

[19] http://www.psi-pci.com/Data_Sheets_Library/DS445.pdf

[20] http://www.torayca.com/techref/en/images/fcp02.html

[21] http://www.toraycfa.com/pdfs/T1000GDataSheet.pdf

[22] http://asm.matweb.com/search/SpecificMaterial.asp?bassnum=MTA321

[23] Madhavi, M., V. J. Rao, and K N. Rao. "Design and analysis of filament wound composite pressure vessel with integrated-end domes." *Defence Science Journal* 59, no. 1 (2009): 73-81.

[24] Juvinall, R.C., and Marshek, K.M. *Fundamentals of machine component design.* Wiley, 2006, p. 214.

[25] Kawahara, G., and S. McCleskey. "Titanium Lined, Carbon Composite Overwrapped Pressure Vessel." *American Institute of Aeronautics & Astronautics* 96, no. 2751 (1996)